Description of the proton and neutron radiative capture reactions in the Gamow shell model

K. Fossez,[1] N. Michel,[1] M. Płoszajczak,[1] Y. Jaganathen,[2,3] and R. M. Id Betan[4,5]
[1]*Grand Accélérateur National d'Ions Lourds (GANIL), CEA/DSM - CNRS/IN2P3, BP 55027, F-14076 Caen Cedex, France*
[2]*Department of Physics & Astronomy, University of Tennessee, Knoxville, Tennessee 37996, USA*
[3]*NSCL/FRIB Laboratory, Michigan State University, East Lansing, Michigan 48824, USA*
[4]*Physics Institute of Rosario (CONICET), Boulevard 27 de Febrero 210 bis, S2000EZP Rosario, Argentina*
[5]*Department of Physics and Chemistry FCEIA(UNR), Avenida Pellegrini 250, S2000BTP Rosario, Argentina*
(Received 5 February 2015; published 16 March 2015)

We formulate the Gamow shell model (GSM) in coupled-channel (CC) representation for the description of proton/neutron radiative capture reactions and present the first application of this new formalism for the calculation of cross sections in mirror reactions ^{7}Be$(p,\gamma)^{8}$B and ^{7}Li$(n,\gamma)^{8}$Li. The GSM-CC formalism is applied to a translationally invariant Hamiltonian with an effective finite-range two-body interaction. Reactions channels are built by GSM wave functions for the ground state $3/2^{-}$ and the first excited state $1/2^{-}$ of ^{7}Be/^{7}Li and the proton/neutron wave function expanded in different partial waves.

DOI: 10.1103/PhysRevC.91.034609 PACS number(s): 21.60.Cs, 03.65.Nk, 24.10.Cn, 25.40.Lw

I. INTRODUCTION

The description of nuclear structure and reactions in the unified theoretical framework is the long-standing challenge of nuclear theory. The attempts to reconcile the shell model (SM) with the reaction theory [1,2] inspired the development of the continuum shell model (CSM) [3] which evolved into the unified of theory of nuclear structure and reactions [3–7].

The structure of weakly bound states and resonances is different from that of well bound states. A comprehensive description of these systems goes beyond standard configuration interaction model such as the SM and requires an open quantum system formulation of the many-body system. Such a generalization of the standard SM to describe well bound, weakly bound, and unbound many-body states is provided by the Gamow shell model (GSM) [8–10]. GSM offers the most general treatment of couplings between discrete and scattering states. The many-body states in GSM are given by the linear combination of Slater determinants defined in the Berggren ensemble of single-particle states which consists of Gamow (resonant) states and the nonresonant continuum.

In this formulation, GSM is the tool par excellence for studies of the structure of bound and unbound many-body states and their decays. For the description of reactions, the GSM has to be formulated in the CC representation. Recently, the GSM-CC approach has been applied for the calculation of excited states of ^{18}Ne and ^{19}Na, excitation functions, and the elastic/inelastic differential cross sections in the ^{18}Ne(p,p') reaction at different energies [11,12] (see also Ref. [13] for the studies of isobaric analog resonances). In this work, we apply the GSM-CC formalism for the description of low-energy radiative capture reactions: ^{7}Be$(p,\gamma)^{8}$B and ^{7}Li$(n,\gamma)^{8}$Li. In light nuclei, GSM-CC can be applied also for the description of nuclear reactions in the *ab initio* framework of the no-core GSM [14] and to heavier projectiles like the α particle.

The solution of solar neutrino problem requires an understanding of the ^{7}Be$(p,\gamma)^{8}$B proton capture reaction. ^{8}B produced in the solar interior in this reaction is the principal source of high energy neutrinos detected in solar neutrino experiments. At the solar energies ($\sim$20 keV), this cross section is too small to be directly measurable. For this reason, the theoretical analysis of this reaction is so important. On the other hand, whenever the measurement is feasible ($E_{\text{c.m.}} > 150$ keV), the exact value of the capture cross section depends (i) on the normalization obtained indirectly from the ^{7}Li$(d,p)^{8}$Li cross section, and (ii) on the model-dependent extrapolation of measured values of the cross section down to the interesting domain of solar energies.

Proton radiative capture reaction on ^{7}Be is of particular importance in astrophysics since it is involved in the pp-II and pp-III reaction chains. Indeed, the relative rates of the ^{7}Be$(e^{-},\nu_{e})^{7}$Li reaction and the ^{7}Be$(p,\gamma)^{8}$B reaction determine the pp-I/pp-II branching ratio, and thus the ratio of the neutrino fluxes coming from ^{7}Be and ^{8}B [15]. The ^{7}Be$(p,\gamma)^{8}$B reaction has been studied experimentally by the direct proton capture [16–26] and the Coulomb dissociation of ^{8}B [27–31]. Theoretical approaches used to describe this reaction include the potential model [32], the R-matrix approach [33,34], the shell model embedded in the continuum (SMEC) [35], the microscopic cluster model [36], and the approach combining the resonating-group method and the no-core shell model [37].

^{7}Li$(n,\gamma)^{8}$Li reaction is the mirror reaction of ^{7}Be$(p,\gamma)^{8}$B. The ^{7}Li$(n,\gamma)^{8}$Li reaction cross section at very low energies provides the essential element of a rapid process of primordial nucleosynthesis of nuclei with $A \geqslant 12$ in the inhomogeneous big-bang models [38–41]. Indeed, in the inhomogeneous big-bang hypothesis, the main reaction chain leading to the synthesis of heavy elements is [40] $^{1}\text{H}(n,\gamma) \rightarrow {}^{2}\text{H}(n,\gamma) \rightarrow {}^{3}\text{H}(d,n) \rightarrow {}^{4}\text{He}(t,\gamma) \rightarrow {}^{7}\text{Li}(n,\gamma)^{8}\text{Li}$, and then $^{8}\text{Li}(\alpha,n) \rightarrow {}^{11}\text{B}(n,\gamma) \rightarrow {}^{12}\text{B}(\beta^{-}) \rightarrow {}^{12}\text{C}(n,\gamma) \rightarrow {}^{13}\text{C} \rightarrow \cdots$, etc., for heavier nuclei. In this sense, the reaction ^{7}Li$(n,\gamma)^{8}$Li is a key process to bridge the gap of mass $A = 8$ and to produce heavy elements. The reaction ^{7}Li$(n,\gamma)^{8}$Li has been studied experimentally [42–45]. Theoretical studies of this reaction has been done using various potential models [46,47], the SMEC [35], the microscopic cluster model [48] and the halo effective field theory approach [49].

The paper is organized as follows. Section II presents the general formalism of the GSM-CC approach. In Sec. II A, we introduce the translationally invariant GSM Hamiltonian in the cluster-orbital shell model (COSM) variables [50]. The coupled-channel equations of GSM-CC are presented in Sec. II B. The channel states expansion in Berggren basis and the calculation of Hamiltonian matrix elements are discussed in Secs. II C and II D, respectively. In Sec. II E, we discuss how to orthogonalize the channel states, and Sec. II F presents the method of solving the GSM-CC equations derived in this work.

Section III is devoted to the presentation of the nucleon radiative capture formalism in the context of GSM-CC. In particular, the method of calculating matrix elements of the electromagnetic operators is explained in Sec. III A, and the matrix elements themselves are given in the Appendix.

Results of the GSM-CC calculations are discussed in Secs. IV and V for ^{7}Be$(p,\gamma)^8$B and ^{7}Li$(n,\gamma)^8$Li low-energy reactions, respectively. Finally, the main conclusions of this work are summarized in Sec. VI.

II. COUPLED-CHANNEL FORMULATION OF THE GAMOW SHELL MODEL

A. Hamiltonian of the Gamow shell model

Center-of-mass (c.m.) excitations in SM wave functions are removed using the Lawson method [51–53]. In the Gamow shell model (GSM), this method cannot be used because Berggren states are not eigenstates of the harmonic oscillator (HO) potential. To avoid spurious c.m. excitations in GSM wave functions, the GSM Hamiltonian is expressed in the intrinsic nucleon-core coordinates of the COSM [50]:

$$\hat{H} = \sum_{i=1}^{N_{\rm val}} \left(\frac{\hat{\vec{p}}_i^{\,2}}{2\mu_i} + U_c(\hat{r}_i) \right) + \sum_{i<j}^{N_{\rm val}} \left(V(\hat{\vec{r}}_i - \hat{\vec{r}}_j) + \frac{\hat{\vec{p}}_i \cdot \hat{\vec{p}}_j}{M_c} \right), \tag{1}$$

where $N_{\rm val}$ is the number of valence nucleons, M_c is the core mass, and $1/\mu_i = 1/M_c + 1/m_i$, is the reduced mass of the ith nucleon. The single-particle (s.p.) potential $U_c(\hat{r})$, which describes the field of the core acting on each nucleon, is a sum of nuclear and Coulomb terms. The nuclear term is given by a Woods-Saxon (WS) field with a spin-orbit term [9]. The Coulomb field is generated by a Gaussian density of Z_c protons of the core [9]. $V(\hat{\vec{r}}_i - \hat{\vec{r}}_j)$ in Eq. (1) is the two-body interaction which splits into nuclear and Coulomb parts. As in the standard SM, adding and subtracting a one-body mean-field $U(\hat{r}_i)$ to the core Hamiltonian and the two-body interaction, respectively, allows us to recast the GSM Hamiltonian in the form

$$\hat{H} = \hat{U}_{\rm basis} + \hat{T} + \hat{V}_{\rm res}, \tag{2}$$

where the potential $\hat{U}_{\rm basis}$ generates the s.p. basis, the kinetic term is written $\hat{T}$ and the residual interaction is given by $\hat{V}_{\rm res}$:

$$\hat{U}_{\rm basis} = \sum_{i=1}^{N_{\rm val}} [U_c(\hat{r}_i) + U(\hat{r}_i)], \tag{3}$$

$$\hat{V}_{\rm res} = \sum_{i<j}^{N_{\rm val}} \left(V(\hat{\vec{r}}_i - \hat{\vec{r}}_j) + \frac{\hat{\vec{p}}_i \cdot \hat{\vec{p}}_j}{M_c} \right) - \sum_{i=1}^{N_{\rm val}} U(\hat{r}_i). \tag{4}$$

In the present studies, we use the Furutani-Horiuchi-Tamagaki (FHT) finite-range two-body interaction [54,55]:

$$V(\hat{\vec{r}}_i - \hat{\vec{r}}_j) \equiv V_{ij} = V_{ij}^{\rm C} + V_{ij}^{\rm SO} + V_{ij}^{\rm T} + V_{ij}^{\rm Co}. \tag{5}$$

The central potential $V_{ij}^{\rm C}$ is

$$V_{ij}^{\rm C} = \sum_{n=1}^{3} V_{0,n}^{\rm C} e^{-\beta_n^{\rm C} r^2} \left(W_n^{\rm C} + B_n^{\rm C} P^\sigma - H_n^{\rm C} P^\tau - M_n^{\rm C} P^\sigma P^\tau \right), \tag{6}$$

where r is the distance between particles i and j, $\beta_n^{\rm C}$ is the range of Gaussians, P^σ and P^τ are the spin exchange and isospin exchange operators, respectively, and $W_n^{\rm C}$, $B_n^{\rm C}$, $H_n^{\rm C}$, and $M_n^{\rm C}$ are the exchange parameters. The spin-orbit potential $V_{ij}^{\rm SO}$ is

$$V_{ij}^{\rm SO} = \vec{L}\cdot\vec{S} \sum_{n=1}^{2} V_{0,n}^{\rm SO} e^{-\beta_n^{\rm SO} r^2} \left(W_n^{\rm SO} - H_n^{\rm SO} P^\tau \right), \tag{7}$$

where $\vec{L}$ is the relative orbital angular momentum between the two particles and $\vec{S} = \vec{s}_i + \vec{s}_j$ where $\vec{s}_i$, $\vec{s}_j$ are the spins of particles i, j. The tensor potential $V_{ij}^{\rm T}$ is

$$V_{ij}^{\rm T} = O_{\rm T} \sum_{n=1}^{3} V_{0,n}^{\rm T} e^{-\beta_n^{\rm T} r^2} \left(W_n^{\rm T} - H_n^{\rm T} P^\tau \right), \tag{8}$$

where

$$O_{\rm T} = \left(\frac{3(\vec{\sigma}_i\cdot\vec{r})(\vec{\sigma}_j\cdot\vec{r})}{r^2} - \vec{\sigma}_i\cdot\vec{\sigma}_j \right) r^2 \tag{9}$$

and $\vec{\sigma}_i$, $\vec{\sigma}_j$ are the Pauli matrices. The Coulomb potential in the FHT interaction is standard.

It is convenient to rewrite the FHT interaction using projection operators on singlet and triplet states of spin and isospin:

$$V^{\rm C}(r) = \mathcal{V}_{\rm tt}^{\rm C} f_{\rm tt}^{\rm C}(r) \pi_{\rm t}^\sigma \pi_{\rm t}^\tau + \mathcal{V}_{\rm ts}^{\rm C} f_{\rm ts}^{\rm C}(r) \pi_{\rm t}^\sigma \pi_{\rm s}^\tau + \mathcal{V}_{\rm st}^{\rm C} f_{\rm st}^{\rm C}(r) \pi_{\rm s}^\sigma \pi_{\rm t}^\tau + \mathcal{V}_{\rm ss}^{\rm C} f_{\rm ss}^{\rm C}(r) \pi_{\rm s}^\sigma \pi_{\rm s}^\tau, \tag{10}$$

$$V^{\rm SO}(r) = \vec{L}\cdot\vec{S} \left(\mathcal{V}_{\rm tt}^{\rm SO} f_{\rm tt}^{\rm SO}(r) \pi_{\rm t}^\sigma \pi_{\rm t}^\tau + \mathcal{V}_{\rm ts}^{\rm SO} f_{\rm ts}^{\rm SO}(r) \pi_{\rm t}^\sigma \pi_{\rm s}^\tau \right), \tag{11}$$

$$V^{\rm T}(r) = O_{\rm T} \left(\mathcal{V}_{\rm tt}^{\rm T} f_{\rm tt}^{\rm T}(r) \pi_{\rm t}^\sigma \pi_{\rm t}^\tau + \mathcal{V}_{\rm ts}^{\rm T} f_{\rm ts}^{\rm T}(r) \pi_{\rm t}^\sigma \pi_{\rm s}^\tau \right), \tag{12}$$

where $\pi_{\rm s}^\sigma$, $\pi_{\rm t}^\sigma$ are the projection operators on singlet and triplet states of spin:

$$\pi_{\rm s}^\sigma = \tfrac{1}{4} - \vec{s}_i\cdot\vec{s}_j, \quad \pi_{\rm t}^\sigma = \tfrac{3}{4} + \vec{s}_i\cdot\vec{s}_j,$$
$$P^\sigma = \tfrac{1}{2} + 2\vec{s}_i\cdot\vec{s}_j = \pi_{\rm t}^\sigma - \pi_{\rm s}^\sigma. \tag{13}$$

Equations (13) have the same form for projection operators $\pi_{\rm s}^\tau$ and $\pi_{\rm t}^\tau$ on singlet and triplet states of isospin. Functions $f_{\sigma\tau}(r)$ in Eqs. (10)–(12) depend on the parameters $V_{0,n}^\zeta$, W_n^ζ, B_n^ζ, H_n^ζ, M_n^ζ, and β_n^ζ, where ζ stands for superscripts C, SO, and T, which are given in Refs. [54,55]. In this work, we adjust the coupling constants $\mathcal{V}_{aa'}^\zeta$ in Eqs. (10)–(12), where a and a' are indices of either singlet (s) or triplet (t) states.

B. The coupled-channel equations

Nuclear reactions can be conveniently formulated in the CC representation of the Schrödinger equation. The first step

to derive the GSM-CC equations is to expand the GSM eigenstates in the complete basis of channel states $\{|c\rangle\} \equiv \{|c_{\rm proj}; c_{\rm targ}\rangle\}$ which contain information about the structure of the target and the projectile. Indices $c_{\rm proj}$ and $c_{\rm targ}$ denote the sets of quantum numbers associated with the projectile and the target, respectively. The nuclear reaction is then described by the relative motion of target and projectile nuclei and the channel parameters, like angular momenta of the target and the projectile and quantum numbers of the target internal excitations. In the following discussion, the heavy reaction participant is called a "target" and the light one a '"projectile." Obviously, the formulation of reaction theory in the GSM-CC approach does not depend on this arbitrary choice of labels.

The antisymmetric eigenstates of GSM-CC equations,

$$\hat{\mathcal{A}}\,|\Psi\rangle = |\Psi\rangle = \sum\!\!\!\!\!\!\int_c \int_0^\infty dr\, r^2\, \langle r,c|\Psi\rangle\, |r,c\rangle\,, \tag{14}$$

where $\hat{\mathcal{A}}$ is the antisymmetrization operator, can be expanded using the channel basis states: $|r,c\rangle = \hat{\mathcal{A}}(|r\rangle \otimes |c\rangle)$. In the above equation, $\langle r,c|\Psi\rangle$ are the antisymmetrized channel wave functions: $\Psi_c(r) \equiv \langle r,c|\Psi\rangle \equiv u_c(r)r$. Hence

$$|\Psi\rangle = \sum\!\!\!\!\!\!\int_c \int_0^\infty dr\, r^2 \frac{u_c(r)}{r}\, |r,c\rangle\,. \tag{15}$$

GSM-CC equations are obtained by inserting (15) in the Schrödinger equation and then projecting this equation on a given channel basis state $\langle r',c'|$. One obtains

$$\sum\!\!\!\!\!\!\int_c \int_0^\infty dr\, r^2 [H_{c',c}(r',r) - E N_{c',c}(r',r)] \frac{u_c(r)}{r} = 0, \tag{16}$$

where

$$H_{c',c}(r',r) = \langle r',c'|\hat{H}|r,c\rangle \tag{17}$$

and

$$N_{c',c}(r',r) = \langle r',c'|r,c\rangle \tag{18}$$

are the Hamiltonian matrix elements and the norm matrix elements in the channel representation, respectively.

C. Channel states expansion in the Berggren basis

In the present studies, any target state $|c_{\rm targ}\rangle$ is an antisymmetrized state of $A-1$ nucleons:

$$\begin{aligned} |c_{\rm targ}\rangle &= \sum_i \left\langle {\rm SD}_i^{(A-1)} \middle| c_{\rm targ} \right\rangle \left| {\rm SD}_i^{(A-1)} \right\rangle \\ &= \sum_i a_{i,c_{\rm targ}} \left| {\rm SD}_i^{(A-1)} \right\rangle \end{aligned} \tag{19}$$

Slater determinants $|{\rm SD}_i^{(A-1)}\rangle$ are built using a complete set of single-particle states of the Berggren ensemble [56] which includes both resonant states and complex-energy scattering states. In this work, the Berggren ensemble is generated by the real single-particle potential $\hat{U}_{\rm basis}$ acting on valence nucleons, but the analogous complete set of single-particle states can be generated by the complex potential as well [57]. This ensemble is also used to generate the states of the projectile:

$$\begin{aligned} \left|\phi_{i;c_{\rm proj}}\right\rangle &= \hat{\mathcal{A}}\left(\left|\phi_i^{\rm rad}\right\rangle \otimes |c_{\rm proj}\rangle\right) \\ &= \hat{\mathcal{A}}\left(\left|\phi_i^{\rm rad}\right\rangle \otimes |l,s;j,m_j\rangle\right) \end{aligned} \tag{20}$$

where $|\phi_i^{\rm rad}\rangle$ and $|c_{\rm proj}\rangle$ are radial and angular parts, respectively. In this expression, l is the orbital angular momentum of the nucleon, s its spin, j is the total angular momentum, and m_j its projection. Hence, the basis state $|r,c_{\rm proj}\rangle$ of a projectile can be written as

$$|r,c_{\rm proj}\rangle = \sum_i \frac{u_i(r)}{r} \left|\phi_{i;c_{\rm proj}}\right\rangle \tag{21}$$

where $u_i(r)/r = \langle \phi_i^{\rm rad}|r\rangle$. Using Eq. (21), one can write the channel basis states as

$$|r,c\rangle = \sum_i \frac{u_i(r)}{r} \left|\phi_i^{\rm rad},c\right\rangle, \tag{22}$$

where $|\phi_i^{\rm rad},c\rangle = \hat{\mathcal{A}}(|\phi_i^{\rm rad}\rangle \otimes |c\rangle)$.

D. Hamiltonian matrix elements

Matrix elements of the Hamiltonian $H_{c',c}(r',r)$ and the norm $N_{c',c}(r',r)$ can be derived using the expansion (22) which allows us to treat the antisymmetry in the projectile-target system. In practice, only a finite number of Slater determinants contribute significantly to the target state, and thus the antisymmetry between the low-energy target states and the high-energy projectile states can be neglected in most cases. The high-energy terms correspond to the channel basis states with high momentum k or high-i indices $i > i_{\rm max}$, where $i_{\rm max}$ depends on the considered channel c. Hence, the expansion (22) can be split into low- and high-energy parts:

$$\begin{aligned} |r,c\rangle &= \sum_{i=1}^{i_{\rm max}-1} \frac{u_i(r)}{r} \left|\phi_i^{\rm rad},c\right\rangle + \sum_{i=i_{\rm max}}^{N} \frac{u_i(r)}{r} \left|\phi_i^{\rm rad},c\right\rangle \\ &\simeq \sum_{i=1}^{i_{\rm max}-1} \frac{u_i(r)}{r} \left|\phi_i^{\rm rad},c\right\rangle + \sum_{i=i_{\rm max}}^{N} \frac{u_i(r)}{r} \left|\phi_i^{\rm rad}\right\rangle \otimes |c\rangle\,, \end{aligned} \tag{23}$$

where N is the number of discretized continuum states and $i_{\rm max}$ is the index from which the antisymmetry effects are neglected. Equivalently, Eq. (23) can be written as

$$\begin{aligned} |r,c\rangle = &\sum_{i=1}^{i_{\rm max}-1} \frac{u_i(r)}{r} \left|\phi_i^{\rm rad},c\right\rangle + |r\rangle \otimes |c\rangle \\ &- \sum_{i=1}^{i_{\rm max}-1} \frac{u_i(r)}{r} \left|\phi_{i;c_{\rm proj}}\right\rangle \otimes |c_{\rm targ}\rangle\,, \end{aligned} \tag{24}$$

where $|r\rangle \otimes |c\rangle$ and $|\phi_{i;c_{\rm proj}}\rangle \otimes |c_{\rm targ}\rangle$ stand for non-antisymmetrized states. In this particular case ($i \geqslant i_{\rm max}$), the GSM Hamiltonian (2) splits into $\hat{H}_{\rm proj}$ and $\hat{H}_{\rm targ}$ terms acting on projectile states $|\phi_{i;c_{\rm proj}}\rangle$ and target states $|c_{\rm targ}\rangle$, respectively. Moreover,

$$\hat{H}_{\rm proj} \left|\phi_{i;c_{\rm proj}}\right\rangle = E_{i,c_{\rm proj}} \left|\phi_{i;c_{\rm proj}}\right\rangle, \tag{25}$$

$$\hat{H}_{\rm targ}\, |c_{\rm targ}\rangle = E_{c_{\rm targ}}\, |c_{\rm targ}\rangle\,. \tag{26}$$

Matrix elements of the Hamiltonian,

$$H_{c',c}(r',r) = \left\langle \phi^{\rm rad}_{i'},c' \middle| \hat{H} \middle| \phi^{\rm rad}_{i},c \right\rangle = \sum_{i,i'=1}^{N} \frac{u_{i'}(r')}{r'} \frac{u_i(r)}{r} H_{c',c}(i',i), \quad (27)$$

and of the norm,

$$N_{c',c}(r',r) = \left\langle \phi^{\rm rad}_{i'},c' \middle| \phi^{\rm rad}_{i},c \right\rangle = \sum_{i,i'=1}^{N} \frac{u_{i'}(r')}{r'} \frac{u_i(r)}{r} N_{c',c}(i',i), \quad (28)$$

are evaluated using the expansion (24).

In the calculation of sums in Eqs. (27) and (28), four cases have to be considered. In the first case, $i < i_{\rm max}$ and $i' < i_{\rm max}$, the matrix elements are calculated in terms of Slater determinants to take into account the antisymmetry. In the second and third cases, $i < i_{\rm max}$ and $i' \geqslant i_{\rm max}$ and $i \geqslant i_{\rm max}$ and $i' < i_{\rm max}$ which are symmetric with respect to the exchange of i and i', the matrix elements are equal to zero because Berggren states $|\phi_{i;c_{\rm proj}}\rangle$ and $|\phi_{i';c_{\rm proj}}\rangle$ with $i \geqslant i_{\rm max}$ or $i' \geqslant i_{\rm max}$ are orthogonal to all target states. In the last case, $i \geqslant i_{\rm max}$ and $i' \geqslant i_{\rm max}$, there is no antisymmetry and only terms with $i = i'$ are nonzero. One obtains,

$$H_{c',c}(r',r) = -\frac{\hbar^2}{2\mu}\left(\frac{1}{r}\frac{\partial^2(r\cdot)}{\partial r^2} - \frac{l(l+1)}{r^2} - k^2_{c_{\rm targ}}\right) \times \frac{\delta(r-r')}{r^2}\delta_{c'_{\rm targ},c_{\rm targ}} + V_{c',c}(r',r), \quad (29)$$

where $k^2_{c_{\rm targ}} = 2\mu E_{c_{\rm targ}}/\hbar^2$ and the channel-channel coupling potential $V_{c',c}(r',r)$ is given by

$$V_{c',c}(r',r) = U_{\rm basis}(r)\frac{\delta(r-r')}{r^2}\delta_{c'_{\rm targ},c_{\rm targ}} + \tilde{V}_{c',c}(r',r) \quad (30)$$

with

$$\tilde{V}_{c',c}(r',r) = \sum_{i,i'=1}^{i_{\rm max}} \frac{u_{i'}(r')}{r'}\frac{u_i(r)}{r} H_{c',c}(i',i) - \sum_{i=1}^{i_{\rm max}-1} \frac{u_i(r')}{r'}\frac{u_i(r)}{r}\left(E_{i,c_{\rm proj}}\delta_{c'_{\rm targ},c_{\rm targ}} + E_{c_{\rm targ}}\right). \quad (31)$$

In the same way, for $N_{c',c}(r',r)$ one obtains

$$N_{c',c}(r',r) = \frac{\delta(r-r')}{r^2}\delta_{c'_{\rm targ},c_{\rm targ}} + \tilde{N}_{c',c}(r',r) \quad (32)$$

with

$$\tilde{N}_{c',c}(r',r) = \sum_{i,i'=1}^{i_{\rm max}} \frac{u_{i'}(r')}{r'}\frac{u_i(r)}{r} N_{c',c}(i',i) - \sum_{i=1}^{i_{\rm max}-1} \frac{u_i(r')}{r'}\frac{u_i(r)}{r}\delta_{c'_{\rm targ},c_{\rm targ}}. \quad (33)$$

E. Orthogonalization of the channel states

The CC formalism leads to a generalized eigenvalue problem because different channel basis states are nonorthogonal. The nonorthogonality of channel states comes from the antisymmetry between the projectile and target states. To formulate GSM-CC equations as the generalized eigenvalue problem, one should express Eq. (16) in the orthogonal channel basis $\{|r,c\rangle_o\}$:

$${}_o\langle r',c'|r,c\rangle_o = \frac{\delta(r'-r)}{r^2}\delta_{c'c}\,. \quad (34)$$

The transformation from the nonorthogonal channel basis $\{|r,c\rangle\}$ to the orthogonal one $\{|r,c\rangle_o\}$ is given by the overlap operator $\hat{O}$ such that $|r,c\rangle = \hat{O}^{\frac{1}{2}}|r,c\rangle_o$. The CC equations (16) written in the orthogonal basis are

$$\sum\!\!\!\!\!\!\int_c \int_0^\infty dr\, r^2 ({}_o\langle r',c'|\hat{H}_o|r,c\rangle_o - E\,{}_o\langle r',c'|\hat{O}|r,c\rangle_o)_o\langle r,c|\Psi_o\rangle = 0, \quad (35)$$

where ${}_o\langle r',c'|\hat{H}_o|r,c\rangle_o = \langle r',c'|\hat{H}|r,c\rangle$, ${}_o\langle r',c'|\hat{O}|r,c\rangle_o = \langle r',c'|r,c\rangle$, and ${}_o\langle r,c|\Psi_o\rangle = \langle r,c|\Psi\rangle$. The transformation of this generalized eigenvalue problem into a standard eigenvalue problem is achieved with a substitution: $|\Phi\rangle = \hat{O}\,|\Psi\rangle$. One obtains:

$$\sum\!\!\!\!\!\!\int_c \int_0^\infty dr\, r^2 ({}_o\langle r',c'|\hat{H}|r,c\rangle_o - E\,{}_o\langle r',c'|r,c\rangle_o)_o\langle r,c|\Phi\rangle = 0 \quad (36)$$

with ${}_o\langle r,c|\Phi\rangle = \langle r,c|\hat{O}^{\frac{1}{2}}|\Psi\rangle \equiv w_c(r)r$. In the nonorthogonal channel basis, these CC equations become

$$\sum\!\!\!\!\!\!\int_c \int_0^\infty dr\, r^2\, \langle r',c'|\hat{H}_m|r,c\rangle \frac{w_c(r)}{r} = E\frac{w_{c'}(r')}{r'}, \quad (37)$$

with ${}_o\langle r',c'|\hat{H}|r,c\rangle_o \equiv \langle r',c'|\hat{H}_m|r,c\rangle$, where $\hat{H}_m = \hat{O}^{-\frac{1}{2}}\hat{H}\hat{O}^{-\frac{1}{2}}$ is the modified Hamiltonian.

Matrix elements of $\hat{H}_m$ are calculated using the expansion (24) as described in Sec. II D. In order to have a more precise treatment of the antisymmetry in the calculation of matrix elements of $\hat{H}_m$, we introduce a new operator $\hat{\Delta}$: $\hat{O}^{-\frac{1}{2}} = \hat{\Delta} + \hat{\mathbf{1}}$, which is associated with the part of $\hat{O}^{-\frac{1}{2}}$ acting on the low-energy channel states. Then, instead of calculating the matrix elements of $\hat{H}_m$ directly, it is possible to calculate them as

$$H_m = (\Delta + \hat{\mathbf{1}})H(\Delta + \hat{\mathbf{1}}) = H + H\Delta + \Delta H + \Delta H \Delta. \quad (38)$$

In this formulation, the non-antisymmetrized terms are taken into account exactly with the identity operator. Inserting (38) in CC equations (37) and replacing matrix elements $\langle r',c'|\hat{H}|r,c\rangle$ using (29) and (30), one obtains the CC equations for the

reduced radial wave functions $w_c(r)/r$:

$$\left[-\frac{\hbar^2}{2\mu}\left(\frac{1}{r}\frac{\partial^2(r\cdot)}{\partial r^2}-\frac{l(l+1)}{r^2}\right)+V_c^{(\mathrm{loc})}(r)\right]\frac{w_c(r)}{r}\frac{\delta(r-r')}{r^2}\delta_{c'_{\mathrm{targ}},c_{\mathrm{targ}}}+\sum_{c'}\int_0^\infty dr'\,rr'^2\frac{V_{c,c'}^{(\mathrm{non\text{-}loc})}(r,r')}{rr'}\frac{w_{c'}(r')}{r'}$$
$$=\left(E-E_{c_{\mathrm{targ}}}\right)\frac{\delta(r-r')}{r^2}\frac{w_c(r)}{r}\delta_{c'_{\mathrm{targ}},c_{\mathrm{targ}}} \tag{39}$$

with the local potential $V_c^{(\mathrm{loc})}(r)=U_{\mathrm{basis}}(r)$ which may depend on the channel c, and the nonlocal potential

$$\frac{1}{r'r}V_{c',c}^{(\mathrm{non\text{-}loc})}(r',r)=\tilde{V}_{c',c}(r',r)+\langle r',c'|\hat{H}\hat{\Delta}|r,c\rangle\,\langle r',c'|\hat{\Delta}\hat{H}|r,c\rangle+\langle r',c'|\hat{\Delta}\hat{H}\hat{\Delta}|r,c\rangle\,. \tag{40}$$

The radial channel wave functions $u_c(r)/r$ are then obtained from the solutions of Eq. (39) using the equation

$$\frac{u_c(r)}{r}=\frac{w_c(r)}{r}+\sum_{c'}\int_0^\infty dr'\,r'^2\,\langle r,c|\hat{O}^{\frac{1}{2}}\hat{\Delta}\hat{O}^{\frac{1}{2}}|r',c'\rangle\,\frac{w_{c'}(r')}{r'}. \tag{41}$$

F. Solution of the GSM-CC equations

CC equations (39) contain a nonlocal potential which has to be treated using a generalization of the method of the equivalent potential [12,58]. The basic idea is to find the equivalent local potential $V_{c,c'}^{(\mathrm{eq})}(r)$ and the source term $S_c(r)$ which would replace local $V_c^{(\mathrm{loc})}(r)$ and nonlocal $V_{c,c'}^{(\mathrm{non\text{-}loc})}(r,r')$ potentials in Eq. (39). Such an equivalent potential is defined by

$$V_{c,c'}^{(\mathrm{eq})}(r)=V_c^{(\mathrm{loc})}(r)\delta_{c',c}+\frac{1-F_{c'}(r)}{w_{c'}(r)}\sum_{c'}\int_0^\infty dr'\,V_{c,c'}^{(\mathrm{non\text{-}loc})}(r,r')w_{c'}(r'), \tag{42}$$

and a corresponding source term is

$$S_c(r)=F_{c'}(r)\sum_{c'}\int_0^\infty dr'\,V_{c,c'}^{(\mathrm{non\text{-}loc})}(r,r')w_{c'}(r'). \tag{43}$$

$F_c(r)$ in Eqs. (42) and (43) is the smoothing function:

$$F_c(r)=\exp-\alpha\left|\frac{w_c(r)}{w'_c(r)}\right|^2\left(1-\exp-\alpha\left|\frac{w_c^{\mathrm{asymp}}(r)}{w_c(r)}-1\right|^2\right) \tag{44}$$

to cancel divergences of the equivalent potential $V_{c,c'}^{(\mathrm{eq})}(r)$ close to the zeros of $w_c(r)$. In this expression, $w'_c(r)=w_c(r)/r$, and w_c^{asymp} is the asymptotic form of $w_c(r)$ when $r\sim 0$. Typically, the value of α varies in the interval $10<\alpha<100$.

With these substitutions, the GSM-CC equations (39) become

$$\frac{\partial^2 w_c(r)}{\partial r^2}=\left(\frac{l(l+1)}{r^2}-k_c^2\right)w_c(r)+\frac{2\mu}{\hbar^2}\left(\sum_{c'}V_{c,c'}^{(\mathrm{eq,\,sy})}(r)w_{c'}(r)+S_c^{(\mathrm{sy})}(r)\right), \tag{45}$$

where $k_c^2=2\mu(E-E_{c_{\mathrm{targ}}})/\hbar^2$. Equation (45) are solved iteratively to determine the equivalent potential, the source term, and the mutually orthogonal radial wave functions $w_c(r)$. Starting point for solving these equations is provided by a set of radial channel wave functions $\{w_c(r)\}$ obtained by the diagonalization of GSM-CC equations (37) in the Berggren basis of channels. Diagonalization of CC equations in the Berggren basis was also considered in Ref. [59]. Note that it is numerically more convenient to express the potential $V_{c,c'}^{(\mathrm{non\text{-}loc})}(r,r')$ of Eq. (39) in a basis of harmonic oscillator states, as $V_{c,c'}^{(\mathrm{non\text{-}loc})}(r,r')$ is short-range. For this, it is sufficient to replace all occurrences of Berggren basis functions $u_i(r)/r$ by harmonic oscillator states overlaps $\langle u_i|u_n^{(\mathrm{HO})}\rangle$ in Eqs. (31) and (33), where $|u_n^{(\mathrm{HO})}\rangle$ is a harmonic oscillator state.

III. THE RADIATIVE CAPTURE PROCESS

We now discuss the calculation of proton/neutron radiative capture cross sections using the antisymmetrized initial and final GSM wave functions. The differential cross section for a proton or neutron radiative capture can be calculated from the Fermi golden rule, which relates the cross section to the matrix elements of a transition operator between an initial state $|i\rangle$ of energy E_i and a final state $|f\rangle$ of energy E_f. The

differential cross section is given by

$$\frac{d\sigma}{d\Omega_\gamma} = \frac{1}{8\pi}\left(\frac{k_\gamma}{k}\right)\left(\frac{e^2}{\hbar c}\right)\left(\frac{\mu_u c^2}{\hbar c}\right)\frac{1}{2s+1}\frac{1}{2J_{\rm targ}+1} \times, \sum_{\substack{M_i,M_f,\\ M_{\rm targ},M_L,\\ P,m_s}} \left|\sum_L i^L\sqrt{2\pi(2L+1)}\left(\frac{k_\gamma^L}{k}\right)\sqrt{\frac{L+1}{L}}\frac{P}{(2L+1)!!}D^L_{M_L P}(\varphi_\gamma,\theta_\gamma,0)\,\langle\Psi_f(J_f,M_f)|\hat{\mathcal{M}}_{L,M_L}|\Phi_i(M_i)\rangle\right|^2$$

$$= \frac{1}{8\pi}\left(\frac{k_\gamma}{k}\right)\left(\frac{e^2}{\hbar c}\right)\left(\frac{\mu_u c^2}{\hbar c}\right)\frac{1}{2s+1}\frac{1}{2J_{\rm targ}+1}\sum_{\substack{M_i,M_f,\\ M_{\rm targ},M_L,\\ P,m_s}}\left|\sum_L g^L_{M_L,P}(k,k_\gamma,\varphi_\gamma,\theta_\gamma)\,\langle\Psi_f(J_f,M_f)|\hat{\mathcal{M}}_{L,M_L}|\Phi_i(M_i)\rangle\right|^2, \quad (46)$$

where

$$g^L_{M_L,P}(k,k_\gamma,\varphi_\gamma,\theta_\gamma) = i^L\sqrt{2\pi(2L+1)}\left(\frac{k_\gamma^L}{k}\right) \times \sqrt{\frac{L+1}{L}}\frac{P}{(2L+1)!!}D^L_{M_L P}(\varphi_\gamma,\theta_\gamma,0). \quad (47)$$

In the above expressions, k_γ (in units of fm^{-1}) is the linear momentum of the emitted photon, $k_\gamma = (E_f - E_i)/(\hbar c)$; $e^2/(\hbar c)$ is the electromagnetic coupling constant; k (in units of fm^{-1}) is the linear momentum of the incoming proton in the c.m. reference frame; $\mu_u c^2$ (in MeV) is the reduced mass of the projectile; s is the spin of the proton; $J_{\rm targ}$ is the total angular momentum of the target; $P = \pm 1$ is the polarization of the photon; and L and M_L are the multipoles and multipole projections of the photon. Moreover, $D^L_{M_L P}(\varphi_\gamma,\theta_\gamma,0)$ is the Wigner D-matrix depending on the angular variables θ_γ and φ_γ of the photon, and $\hat{\mathcal{M}}_{L,M_L}$ is the electromagnetic transition operator. The final state $|f\rangle$ corresponds to the GSM-CC state $|\Psi_f(J_f,M_f)\rangle$ of a total angular momentum J_f and a projection M_f. The initial state $|i\rangle$ has a fixed value of the total angular momentum projection M_i and is denoted $|\Phi_i(M_i)\rangle$:

$$|\Phi_i(M_i)\rangle = \sum_{J_i,c_e} i^{l_{c_e}} e^{i\sigma_{l_{c_e}}}\sqrt{2l_{c_e}+1}\,|\Psi_i(J_i,M_i,c_e)\rangle \times \left\langle l_{c_e},0,s,m_s\middle|\left(l_{c_e},s\right)j_{c_e},m_s\right\rangle \times \left\langle j_{c_e},m_s,J_{\rm targ},M_{\rm targ}\middle|\left(j_{c_e},J_{\rm targ}\right)J_i,M_i\right\rangle, \quad (48)$$

where $|\Psi_i(J_i,M_i,c_e)\rangle$ is the initial GSM-CC state with a total angular momentum J_i and entrance channel quantum numbers c_e. Each set of quantum numbers c_e corresponds to a different channel c. This state can be expressed in the channel basis as

$$|\Psi_i(J_i,M_i,c_e)\rangle = \sum_c |\Psi_i(J_i,M_i,c_e)\rangle_c\,.$$

Thus, the differential cross section (in units of fm^2) is

$$\frac{d\sigma}{d\Omega_\gamma} = \frac{1}{8\pi}\left(\frac{k_\gamma}{k}\right)\left(\frac{e^2}{\hbar c}\right)\left(\frac{\mu_u c^2}{\hbar c}\right)\frac{1}{2s+1}\frac{1}{2J_{\rm targ}+1} \times \sum_{\substack{M_i,M_f,\\ P,m_s,\\ M_{\rm targ},M_L}}\left|\sum_L g^L_{M_L,P}(k,k_\gamma,\varphi_\gamma,\theta_\gamma)\sum_{J_i,c_e}\langle J_f M_f|\mathcal{M}_{L,M_L}\left|(J_i M_i)_{c_e}\right\rangle\left\langle l_{c_e}0sm_s\middle|j_{c_e}m_s\right\rangle\left\langle j_{c_e}m_s J_{\rm targ}M_{\rm targ}\middle|J_i M_i\right\rangle\right|^2$$

$$= \frac{1}{8\pi}\left(\frac{k_\gamma}{k}\right)\left(\frac{e^2}{\hbar c}\right)\left(\frac{\mu_u c^2}{\hbar c}\right)\frac{1}{2s+1}\frac{1}{2J_{\rm targ}+1}\times\sum_{\substack{M_i,M_f,\\ P,m_s,\\ M_{\rm targ},M_L}}\sum_{\substack{L,L',\\ J_i,J_i',\\ c_e,c_e'}}\left(g^L_{M_L,P}(k,k_\gamma,\varphi_\gamma,\theta_\gamma)g^{L'}_{M_L,P}(k,k_\gamma,\varphi_\gamma,\theta_\gamma)\right.$$
$$\times\langle J_f M_f|\mathcal{M}_{L,M_L}\left|(J_i M_i)_{c_e}\right\rangle\langle J_f M_f|\mathcal{M}_{L',M_L}\left|(J_i' M_i)_{c_e'}\right\rangle\times\left\langle l_{c_e}0sm_s\middle|j_{c_e}m_s\right\rangle\left\langle l_{c_e'}0sm_s\middle|j_{c_e'}m_s\right\rangle$$
$$\left.\times\left\langle j_{c_e}m_s J_{\rm targ}M_{\rm targ}\middle|J_i M_i\right\rangle\left\langle j_{c_e'}m_s J_{\rm targ}M_{\rm targ}\middle|J_i' M_i\right\rangle\right). \quad (49)$$

The operator $\hat{\mathcal{M}}_{L,M_L}$ separates into an electric part $\hat{\mathcal{M}}^E_{L,M_L}$ and a magnetic part $\hat{\mathcal{M}}^M_{L,M_L}$. Formulas for the operators $\hat{\mathcal{M}}^E_{L,M_L}$ and $\hat{\mathcal{M}}^M_{L,M_L}$ are given in the Appendix.

Calculation of many-body matrix elements of the electromagnetic operators

The main difficulty in the calculation of matrix elements comes from the infinite range of the electromagnetic operators

and the antisymmetry of the GSM-CC states. Indeed, direct calculation of these matrix elements in the Berggren basis is not possible because they diverge even using the exterior complex scaling method.

If one neglects antisymmetry in the channel state $|r,c\rangle$,

$$|r,c\rangle = |r\rangle \otimes |c\rangle = |r\rangle \otimes \left[\, |J_{\text{targ},c}, M_{\text{targ},c}\rangle \otimes \left|l_c, s_c; j_c, m_{j_c}\right\rangle\right]^J_M, \quad (50)$$

then the overlap between a bound state or a narrow resonance and a scattering state converges using the exterior complex-scaling method. In the above expression, $J_{\text{targ},c}$ is the angular momentum of the target in a channel c with a projection $M_{\text{targ},c}$, l_c is the orbital momentum of the projectile, s_c its spin and j_c its total angular momentum with a projection m_{j_c}. The antisymmetry between the target and the projectile can be neglected only at large distances because the probability that the one-body state of the projectile is occupied by the target nucleon decreases with the target density. In this case, the action of a given operator $\hat{O}^L_{M_L}$ can be defined by considering target nucleons as distinguishable from the projectile nucleons:

$$\hat{O}^L_{M_L} = \sum_{i\in A} \hat{O}^L_{M_L}(r_i,\Omega_i) + \hat{O}^L_{M_L}(r_{\text{proj}},\Omega_{\text{proj}}). \quad (51)$$

The first sum acts only on target nucleons whereas the second term acts on a projectile. Obviously, this approximation is not valid for a target in the continuum state.

The calculation of matrix elements of the electromagnetic operators goes as follows. The matrix elements are expressed as the sum of a non-antisymmetrized (nas) part and its complement:

$$\langle\Psi_f||\hat{O}^L||\Psi_i\rangle = \langle\Psi_f||\hat{O}^L||\Psi_i\rangle_{\text{nas}} + (\langle\Psi_f||\hat{O}^L||\Psi_i\rangle - \langle\Psi_f||\hat{O}^L||\Psi_i\rangle_{\text{nas}}). \quad (52)$$

The calculation of this complement is achieved by separating the operator $\hat{O}^L$ into a short-range part $\hat{O}^L_<$ and a long-range part $\hat{O}^L_>$. Then the symmetrized and antisymmetrized matrix elements are

$$\langle\Psi_f||\hat{O}^L||\Psi_i\rangle = \langle\Psi_f||\hat{O}^L_<||\Psi_i\rangle + \langle\Psi_f||\hat{O}^L_>||\Psi_i\rangle\,, \quad (53)$$

$$\langle\Psi_f||\hat{O}^L||\Psi_i\rangle_{\text{nas}} = \langle\Psi_f||\hat{O}^L_<||\Psi_i\rangle_{\text{nas}} + \langle\Psi_f||\hat{O}^L_>||\Psi_i\rangle_{\text{nas}}\,. \quad (54)$$

At large distances, the antisymmetry is not crucial and thus the matrix element $\langle\Psi_f||\hat{O}^L_>||\Psi_i\rangle$ can be approximated by $\langle\Psi_f||\hat{O}^L_>||\Psi_i\rangle_{\text{nas}}$. The remaining term is basically a short-range part which can be expanded in the HO basis. One obtains:

$$\langle\Psi_f||\hat{O}^L||\Psi_i\rangle = \langle\Psi_f||\hat{O}^L||\Psi_i\rangle_{\text{nas}} + \langle\Psi_f||\hat{O}^L_<||\Psi_i\rangle^{\text{HO}} - \langle\Psi_f||\hat{O}^L_<||\Psi_i\rangle^{\text{HO}}_{\text{nas}}\,. \quad (55)$$

The matrix element $\langle\Psi_f||\hat{O}^L||\Psi_i\rangle_{\text{nas}}$ is not antisymmetrized. We may write the operator $\hat{O}^L$ [Eq. (51)] as $\hat{O}^L_{\text{targ}} + \hat{O}^L_{\text{proj}}$, where $\hat{O}^L_{\text{targ}}$ acts only on the target state and $\hat{O}^L_{\text{proj}}$ on the projectile state. In this case, matrix elements of the electromagnetic operator acting on target states are

$$\begin{aligned} {}_{c_f}\langle\Psi_f|\big|\hat{O}^L_{\text{targ}}\big||\Psi_i\rangle_{c_i} &= \int_0^\infty dr\, r^2 \frac{u_{c_f}(r)}{r} \int_0^\infty dr'\, r'^2 \frac{u_{c_i}(r')}{r'} \langle r|r'\rangle \left\langle l_{c_f}, s_{c_f}; j_{c_f}, m_{j_{c_f}} \middle| l_{c_i}, s_{c_i}; j_{c_i}, m_{j_{c_i}} \right\rangle \left\langle J_{T_{c_f}} \middle|\middle| \hat{O}^L_{\text{targ}} \middle|\middle| J_{T_{c_i}} \right\rangle \\ &= (-1)^{J_{T_f}+j_f+J_i+L} \sqrt{(2J_f+1)(2J_i+1)} \begin{Bmatrix} J_{T_f} & J_{T_i} & L \\ J_i & J_f & j_i \end{Bmatrix} \left\langle J_{T_f}||\hat{O}^L||J_{T_i}\right\rangle \delta_{l_i l_f} \delta_{j_i j_f} \int_0^\infty dr\, u_{c_f}(r) u_{c_i}(r), \end{aligned} \quad (56)$$

where $\langle r|r'\rangle = \delta_{r,r'}/r^2$, and c_i and c_f denote initial and final channels, respectively. No exterior complex scaling is necessary to calculate the radial overlap in the above expression because $u_{c_i}(r)$ is the scattering wave function of a real energy and $u_{c_f}(r)$ is the bound state wave function. Similarly, matrix elements of the electromagnetic operator acting on the projectile states are

$$\begin{aligned} {}_{c_f}\langle\Psi_f|\big|\hat{O}^L_{\text{proj}}\big||\Psi_i\rangle_{c_i} &= \int_0^\infty dr\, r^2 \frac{u_{c_f}(r)}{r} \int_0^\infty dr'\, r'^2 \frac{u_{c_i}(r')}{r'} \langle r|r'\rangle \left\langle J_{T_{c_f}}, M_{T_{c_f}} \middle| J_{T_{c_i}}, M_{T_{c_i}} \right\rangle \left\langle \left(l_{c_f}, s_{c_f}\right) j_{c_f} \middle|\middle| \hat{O}^L_{\text{proj}} \middle|\middle| \left(l_{c_i}, s_{c_i}\right) j_{c_i} \right\rangle \\ &= \delta_{T_i T_f} (-1)^{J_{T_i}+j_i+J_f+L} \sqrt{(2J_f+1)(2J_i+1)} \begin{Bmatrix} j_f & j_i & L \\ J_i & J_f & J_{T_i} \end{Bmatrix} \left\langle u_{c_f}, \left(l_{c_f}, s\right) j_{c_f} \middle|\middle| \hat{O}^L \middle|\middle| u_{c_i}, \left(l_{c_i}, s\right) j_{c_i} \right\rangle. \end{aligned} \quad (57)$$

The antisymmetrized matrix elements $\langle\Psi_f||\hat{O}^L||\Psi_i\rangle^{\text{HO}}$ in Eq. (55) are obtained by expressing Berggren basis states in the HO basis. In this case, the reduced radial wave functions $u_c(r)$ can be written as

$$\frac{u_c(r)}{r} = \langle r|u_c\rangle \to \sum_n \langle r|u_n\rangle \langle u_n|u_c\rangle = \sum_n u_n(r) \langle u_n|u_c\rangle = \left\langle r \middle| u^{\text{HO}}_c \right\rangle = \frac{u^{\text{HO}}_c(r)}{r}, \quad (58)$$

where $|u_n\rangle$ is the radial HO state and the channel state $|r,c\rangle$ can be expressed as

$$|r,c\rangle = \hat{\mathcal{A}}(|r\rangle \otimes |c\rangle) = \hat{\mathcal{A}}\left(\left(\sum_n \langle u_n|r\rangle\, |u_n\rangle\right) \otimes |c\rangle\right) = \sum_n \langle u_n|r\rangle\, |u_n, c\rangle = \sum_n \frac{u^{\text{HO}}_n(r)}{r} |u_n, c\rangle \quad (59)$$

with $|u_n,c\rangle = [\hat{a}^\dagger_{n,j_c,m_{j_c}}|J_{\text{targ},c},M_{\text{targ},c}\rangle]^J_M$. Hence, the CC representation of initial and final states in HO basis is

$$|\Psi\rangle^{\text{HO}} = \sum_c \sum_n \langle u_n|u_c^{\text{HO}}\rangle |u_n,c\rangle \tag{60}$$

and the antisymmetrized matrix elements of the electromagnetic operator are

$$^{\text{HO}}\langle\Psi_f||\hat{O}^L||\Psi_i\rangle^{\text{HO}} = \sum_{c_i,c_f}\sum_{n_i,n_f}\langle u_{c_i}^{\text{HO}}|u_{n_i}\rangle\langle u_{n_f}|u_{c_f}^{\text{HO}}\rangle \times \left[\langle J_{T_{c_f}}|\hat{a}_{n_f,j_{c_f}}\right]^J_M \hat{O}^L_{M_L}\left[\hat{a}^\dagger_{n_i,j_{c_i}}|J_{T_{c_i}}\rangle\right]^J_M. \tag{61}$$

HO expansion is hereby justified by the fact that the target states are localized.

The last many-body matrix element in Eq. (55), $^{\text{HO}}\langle\Psi_f||\hat{O}^L||\Psi_i\rangle^{\text{HO}}_{\text{nas}}$, is calculated using Eqs. (56) and (57) and replacing $u_c(r)$ by $u_c^{\text{HO}}(r)$ [see Eq. (58)].

IV. RESULTS OF GSM-CC CALCULATIONS FOR THE ^{7}Be$(p,\gamma)^8$B REACTION

GSM-CC calculations are done in COSM coordinates but the radiative capture cross section is expressed in the c.m. reference frame. The initial energy is $E_i^{(\text{COSM})} = E_{\text{proj}}^{(\text{COSM})} + E_T^{(\text{COSM})}$, where $E_i^{(\text{COSM})}$, $E_{\text{proj}}^{(\text{COSM})}$, and $E_T^{(\text{COSM})}$ are the total energy, the projectile energy, and the GSM target binding energy, respectively. All energies are calculated in the COSM coordinate system. The link between the projectile energies in COSM and c.m. reference frames is given by

$$E_{\text{proj}}^{(\text{COSM})} = E_{\text{proj}}^{(\text{c.m.})}\frac{A}{A-1} = \frac{\hbar^2\left(k_{\text{proj}}^{(\text{c.m.})}\right)^2}{2m_p}\frac{A}{A-1}, \tag{62}$$

where $k_{\text{proj}}^{(\text{c.m.})}$ is the linear momentum of the projectile. Energy conservation implies that the final energy is $E_i^{(\text{COSM})} = E_f^{(\text{COSM})} + E_\gamma$, where $E_f^{(\text{COSM})}$ is the compound system binding energy in the COSM frame of reference, and $E_\gamma = k_\gamma\hbar c$ is the photon energy which does not depend on the chosen reference frame.

Resonances in the spectrum of a composite A-nucleon system correspond to the peaks in the radiative capture cross section at the c.m. energy, $E_{\text{c.m.}} = E_i^{(A)}[\text{GSM-CC}] - E_0^{(A-1)}[\text{GSM}]$. Here $E_i^{(A)}[\text{GSM-CC}]$ is the GSM-CC energy of the resonance i in the nucleus A, and $E_0^{(A)}[\text{GSM}]$ is the GSM ground state energy of the target nucleus $(A-1)$.

The cross section for a final state of the total angular momentum J_f is

$$\sigma_{J_f}(E_{\text{c.m.}}) = \int_0^{2\pi} d\varphi_\gamma \int_0^\pi \sin\theta_\gamma d\theta_\gamma \frac{d\sigma_{J_f}(E_{\text{c.m.}},\theta_\gamma,\varphi_\gamma)}{d\Omega\gamma} \tag{63}$$

and the total cross section is thus

$$\sigma(E_{\text{c.m.}}) = \sum_{J_f}\sigma_{J_f}(E_{\text{c.m.}}). \tag{64}$$

TABLE I. Parameters of the WS potential of the ^{4}He core used in the GSM and GSM-CC description of ^{7}Be and ^{8}B.

Parameter	Protons	Neutrons
a	0.65 fm	0.65 fm
R_0	2.0 fm	2.0 fm
$V_{\text{o}}(l=0)$	61.5 MeV	70.6735 MeV
$V_{\text{so}}(l=0)$	0 MeV	0 MeV
$V_{\text{o}}(l=1)$	44.3967 MeV	70.6734 MeV
$V_{\text{so}}(l=1)$	7.80188 MeV	7.86276 MeV
$V_{\text{o}}(l=2)$	44.3967 MeV	0 MeV
$V_{\text{so}}(l=2)$	7.80188 MeV	0 MeV

In practice, one often shows the astrophysical factor

$$S(E_{\text{c.m.}}) = \sigma(E_{\text{c.m.}})E_{\text{c.m.}}e^{2\pi\eta}, \tag{65}$$

which removes the exponential dependence of the cross section at low energies due to the Coulomb barrier. η in Eq. (65) is the Sommerfeld parameter, $\eta = (mZ_1Z_2)/(\hbar^2k)$, where Z_1 and Z_2 are the proton numbers of the projectile and target nuclei.

A. Parameters of GSM calculations in ^{7}Be and ^{8}B

The model space in ^{7}Be and ^{8}B is limited by the core of ^{4}He. The core is described by a WS potential (see Table I) for each considered partial wave: $l = 0$, 1, and 2. The radius of the Coulomb potential is $r_c = 2.8$ fm. To determine Berggren ensemble, one calculates first the single-particle bound and resonance states of the basis generating WS potential for all chosen partial waves (l,j). Then, for each (l,j), one selects the contour $\mathcal{L}^+_{lj}$ in a fourth quadrant of the complex k plane. All (l,j)-scattering states in this ensemble belong to $\mathcal{L}^+_{lj}$. The precise form of the contour is unimportant providing that all selected single-particle resonances for a given (l,j) lie between this contour and the real k axis for $\mathcal{R}(k) > 0$. For each (l,j), the set of all resonant states and scattering states on $\mathcal{L}^+_{lj}$ forms a complete single-particle basis.

In the present case, valence nucleons can occupy the $0p_{3/2}$ and $0p_{1/2}$ discrete single-particle states and several nonresonant single-particle continuum states on discretized contours: $\mathcal{L}^+_{s_{1/2}}$, $\mathcal{L}^+_{p_{1/2}}$, $\mathcal{L}^+_{p_{3/2}}$, $\mathcal{L}^+_{d_{3/2}}$, and $\mathcal{L}^+_{d_{5/2}}$. Each contour consists of three segments joining the points: $k_{\text{min}} = 0.0$, $k_{\text{peak}} = 0.15 - i0.14$ fm^{-1}, $k_{\text{middle}} = 0.3$ fm^{-1} and $k_{\text{max}} = 2.0$ fm^{-1}, and each segment is discretized with 10 points. Hence, GSM and GSM-CC calculations are done in 152 shells: 31 $p_{3/2}$ and $p_{1/2}$ shells, and 30 $s_{1/2}$, $d_{3/2}$, and $d_{5/2}$ shells. The GSM basis is truncated so as to reduce the size of the GSM Hamiltonian matrix. For this, the occupation of $p_{3/2}$ and $p_{1/2}$ scattering states in basis Slater determinants is limited to two particles, while the occupation of $s_{1/2}$, $d_{5/2}$, and $d_{3/2}$ scattering states is limited to one particle only. The latter truncation is justified by the fact that GSM target states virtually only consists of $p_{3/2}$ and $p_{1/2}$ states, $s_{1/2}$, $d_{5/2}$, and $d_{3/2}$ states occurring only in the partial wave decomposition of the proton or neutron projectile.

Parameters of the Hamiltonian, which were adjusted to reproduce binding energies of low-lying states in ^{7}Be and ^{8}B, are given in Table II. In GSM calculations, the ground state of ^{7}Be is bound with respect to ^{4}He by 9.378 MeV, close to

TABLE II. Parameters of the FHT interaction in GSM and GSM-CC calculations in ^{7}Be and ^{8}B. The superscripts C, SO, and T stand for central, spin-orbit, and tensor, respectively, and the indices "s" and "t" stand for singlet and triplet.

Parameter	Value (MeV)
$\mathcal{V}^{\rm C}_{\rm t,t}$	4.00906
$\mathcal{V}^{\rm C}_{\rm s,t}$	–3.22579
$\mathcal{V}^{\rm C}_{\rm s,s}$	2.22077
$\mathcal{V}^{\rm C}_{\rm t,s}$	–9.51008
$\mathcal{V}^{\rm SO}_{\rm t,t}$	–1448.32
$\mathcal{V}^{\rm SO}_{\rm s,t}$	0
$\mathcal{V}^{\rm T}_{\rm t,t}$	15.3946
$\mathcal{V}^{\rm T}_{\rm s,t}$	–15.4834

the experimental value $E_{\rm exp} = 9.304$ MeV. Reaction channels in GSM-CC calculations are obtained by the coupling of the ground state $3/2^-$ and the first excited state $1/2^-$ of ^{7}Be with the proton partial waves: $s_{1/2}$, $p_{1/2}$, $p_{3/2}$, $d_{3/2}$, and $d_{5/2}$.

Discrete states of a composite system ^{8}B are 2^+_1 bound state, and 1^+_1, 3^+_1, 1^+_2 resonances. Missing reaction channels in GSM-CC lead to a small difference between GSM and GSM-CC energies for these states. To correct this deficiency, the channel-channel coupling potentials $V_{c,c'}$ in GSM-CC have been adjusted for each considered state of ^{8}B. The new potentials are $\tilde{V}_{c,c'} = c(J^\pi)V_{c,c'}$, where the multiplicative corrective factors are $c(2^+_1) = 1.0133$, $c(1^+_1) = 1.0602$, and $c(3^+_1) = 1.0233$.

B. The astrophysical S factor for the ^{7}Be$(p,\gamma)^8$B reaction

The description of electromagnetic transitions requires effective charges for proton and neutron. For $E1$ transitions, the standard values are [60]

$$e^p_{\rm eff} = e\left(1 - \frac{Z}{A}\right), \quad e^n_{\rm eff} = -e\frac{Z}{A}, \tag{66}$$

where Z and A are the proton number and the total number of nucleons, respectively. The standard values for $E2$ transitions are

$$e^p_{\rm eff} = e\left(1 - \frac{Z}{A} + \frac{Z}{A^2}\right), \quad e^n_{\rm eff} = -e\frac{Z}{A^2}. \tag{67}$$

There are no effective charges for $M1$ transitions. In the present work, we use these standard values for $E1$ and $E2$ effective charges. One should keep in mind, however, that the effective charges extracted experimentally often show significant deviations from the standard values [61].

The proton separation energy in the ground state of ^{7}Be is $S_{\rm p} = 5.6$ MeV. The final nucleus ^{8}B has one weakly bound state 2^+_1 below the proton emission threshold. The experimental proton separation energy in this state, $S_{\rm p} = 0.1375$ MeV, agrees well with the calculated value $S^{\rm (th)}_{\rm p} = 0.137$ MeV. The 1^+_1 and 3^+_1 resonance peaks should be seen in $M1$ transitions. The 1^+_1 resonance could also be seen in $E2$ transitions.

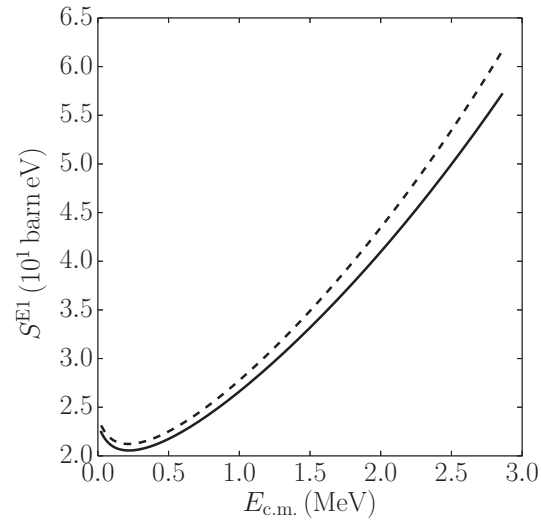

FIG. 1. Plot of the E1 astrophysical factor for the ^{7}Be$(p,\gamma)^8$B reaction. The solid line represents the exact, fully antisymmetrized calculation with both the ground state $J^\pi = 3/2^-_1$ and the first excited state $J^\pi = 1/2^-_1$ of the ^{7}Be target included. The dashed line shows results of the calculations if the first excited state of ^{7}Be is omitted. For more details, see the description in the text.

All relevant $E1$, $M1$, and $E2$ transitions from the initial continuum states ($J_i = 1^+,2^+,3^+$) in ^{8}B to the final bound state $J_f = 2^+$ state have been included. Figures 1–3 show the separate contributions to the total S factor in the ^{7}Be$(p,\gamma)^8$B reaction: S^{E1} for $E1$ transitions (Fig. 1), S^{M1} for $M1$ transitions (Fig. 2), and S^{E2} for $E2$ transitions. The solid lines in Figs. 1–3 show results of the fully antisymmetrized GSM-CC calculations with both ground and first excited states of the ^{7}Be target included. The dashed lines in these figures correspond to GSM-CC calculations neglecting the $1/2^-$ first excited state in ^{7}Be.

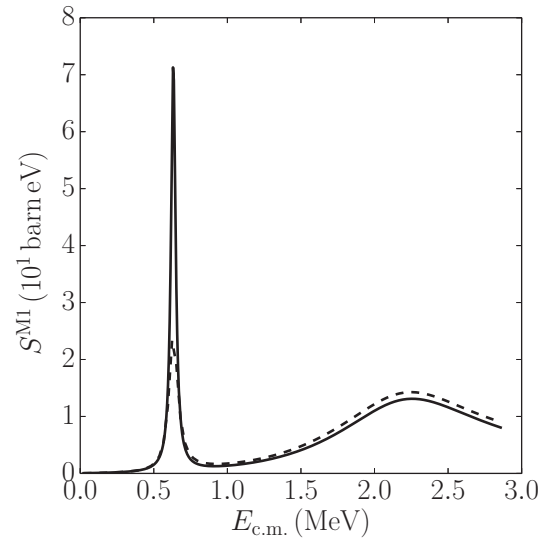

FIG. 2. The same as in Fig. 1 but for the $M1$ transitions. The two peaks correspond to the 1^+_1 and 3^+_1 resonances of ^{8}B.

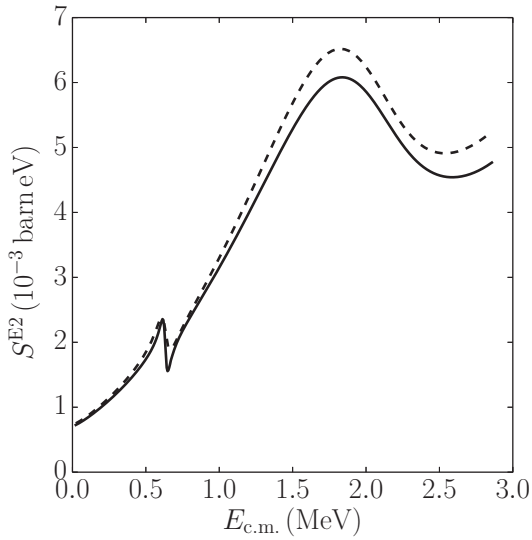

FIG. 3. The same as in Fig. 1 but for the $E2$ transitions. The two peaks correspond to the 1^+_1 and 1^+_2 resonances of ^{8}B.

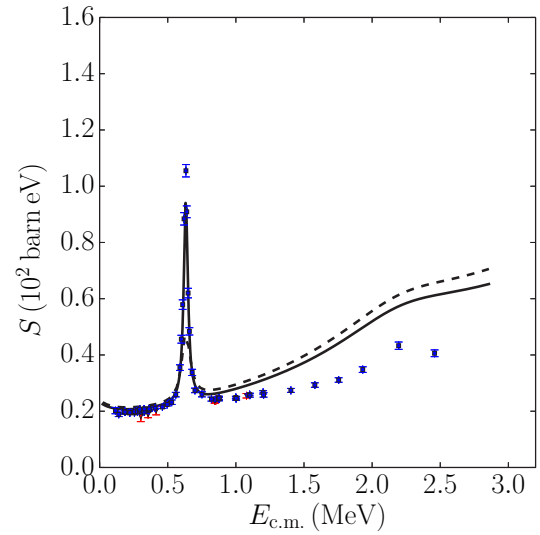

FIG. 4. (Color online) Plot of the total astrophysical factor for the ^{7}Be$(p,\gamma)^8$B reaction. Data are taken from Refs. [22,26]. The solid line represents the exact, fully antisymmetrized calculation including both the ground state $J^\pi = 3/2^-_1$ and the first excited state $J^\pi = 1/2^-_1$ of the ^{7}Be target. Calculations neglecting the first excited state of the target are shown with the dashed line. For more details see the description in the text.

There is no resonant contribution in $E1$ transitions. Including the first excited state of the target lowers S^{E1} by less than $\sim 5\%$ for $E_{c.m.} < 2.5$ MeV. In contrast, the $M1$ contribution to the S factor increases significantly in the region of 1^+_1 resonance if the excited state of the target is included (see Fig. 2). One can see 1^+_1 and 3^+_1 resonances of ^{8}B at $E_{c.m.} = 0.79$ MeV and $E_{c.m.} = 2.34$ MeV, respectively. These resonances are observed experimentally at $E_{c.m.} = 0.632$ MeV and $E_{c.m.} = 2.182$ MeV, respectively. The $E2$ transitions contribute little to the S factor. S^{E2} is $\sim 10^{-3}$ smaller than S^{E1}, and S^{M1} and increases by less than $\sim 10\%$ for c.m. energies in the region of 1^+_1 and 1^+_2 resonances. The resonance 1^+_2 has not yet been seen experimentally.

The calculated total S factor is compared with the experimental data [22,26] in Fig. 4. Below $E_{c.m.} = 1$ MeV, the agreement with the data is good if both the ground state of ^{7}Be and its first excited state are included. The value of the S factor at zero energy, $S^{\mathrm{GSM-CC}}(0)$, is 23.214 b eV and the slope, $\partial S/\partial E_{c.m.}|_{E_{c.m.}=0}$, is 37.921 b. The accepted experimental value of the S factor is 20.9 ± 0.6 b eV, slightly below the GSM-CC results.

At higher energies, GSM-CC results overshoot the experimental data. This feature could be due to the absence of higher lying discrete and continuum states of the ^{7}Be target in the channel basis. Indeed, in the present case, GSM and GSM-CC calculations with uncorrected channel-channel coupling potentials $V_{c,c'}$ do not give the same spectra and binding energies of ^{7}Be and ^{8}B, and the small multiplicative correction factors are necessary.

The long-wavelength approximation simplifies the calculation of matrix elements of the electromagnetic transitions. The quality of this approximation and the role of the antisymmetry of initial and final states is tested in Figs. 5 and 6. Only the ground state of ^{7}Be is taken into account. To correct GSM-CC calculations for the missing channels in this case, the channel-channel coupling potentials $V_{c,c'}$ have been slightly corrected: $\tilde{V}_{c,c'} = c(J^\pi)V_{c,c'}$, and the multiplicative corrective factors are $c(2^+_1) = 1.0122$, $c(1^+_1) = 1.0668$, and $c(3^+_1) = 1.0225$.

At low energies ($E_{c.m.} < 1.5$ MeV), neither the long-wavelength approximation nor the antisymmetrization in the calculation of $E1$ transition matrix elements change the results significantly (see Fig. 5). Both approximations become worse at higher energies but even at $E_{c.m.} = 2.5$ MeV the error is only $\sim 10\%$.

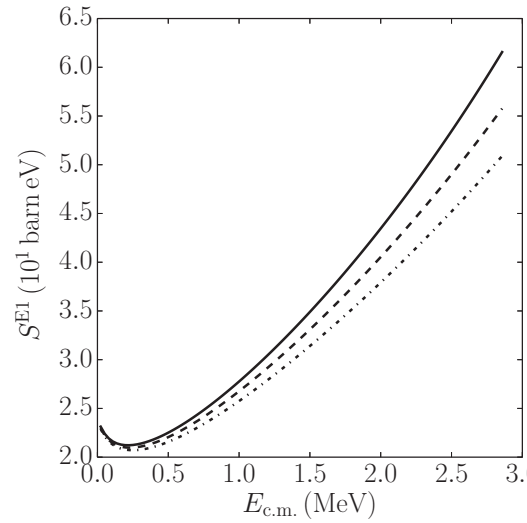

FIG. 5. Plot of the $E1$ astrophysical factor for the ^{7}Be$(p,\gamma)^8$B reaction. The solid line represents the exact, fully antisymmetrized calculation. The calculations in the long-wavelength approximation are represented by the dashed and dotted lines in the fully antisymmetrized and non-antisymmetrized cases, respectively. For more details, see the description in the text.

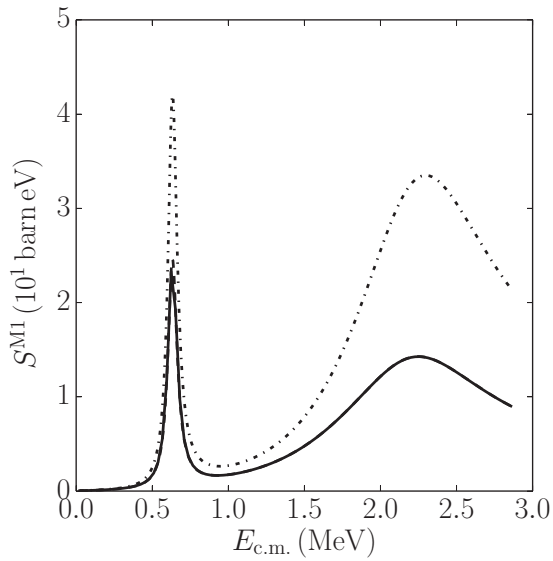

FIG. 6. The same as in Fig. 5 but for the $M1$ transitions. The two peaks correspond to the 1^+_1 and 3^+_1 resonances of ^{8}B.

The astrophysical factor for $M1$ transitions is shown in Fig. 6. The antisymmetrization of the initial and final states lowers the value of S^{M1} by a factor $\sim$2 at the resonance peaks. The long-wavelength approximation does not change S^{M1}.

V. RESULTS OF GSM-CC CALCULATIONS FOR THE ^{7}Li$(n,\gamma)^8$Li REACTION

A. Parameters of GSM calculations in ^{7}Li and ^{8}Li

^{7}Li$(n,\gamma)^8$Li is the mirror reaction of ^{7}Be$(p,\gamma)^8$B and will be described in the same model space. The WS potential of ^{4}He core is given in Table III. The radius of the Coulomb potential is $r_c = 2.8$ fm. Valence nucleons occupy $0p_{3/2}$ and $0p_{1/2}$ discrete single-particle states and nonresonant single-particle continuum states on discretized contours: $\mathcal{L}^+_{s_{1/2}}$, $\mathcal{L}^+_{p_{1/2}}$, $\mathcal{L}^+_{p_{3/2}}$, $\mathcal{L}^+_{d_{3/2}}$, and $\mathcal{L}^+_{d_{5/2}}$. Each contour consists of three segments joining the points: $k_{\rm min} = 0.0$, $k_{\rm peak} = 0.15 - i0.14$ fm^{-1}, $k_{\rm middle} = 0.3$ fm^{-1}, and $k_{\rm max} = 2.0$ fm^{-1}, and each segment is discretized by 10 points.

Parameters of the FHT Hamiltonian in ^{7}Li and ^{8}Li are given in Table IV. In GSM, the ground state of ^{7}Li is bound by 11.228 MeV with respect to ^{4}He, i.e., close to the experimental

TABLE III. Parameters of the WS potential of ^{4}He core used in the GSM and GSM-CC description of ^{7}Li and ^{8}Li nuclei.

Parameter	Protons	Neutrons
a	0.65 fm	0.65 fm
R_0	2.0 fm	2.0 fm
$V_{\rm o}(l=0)$	71.0752 MeV	43.6438 MeV
$V_{\rm so}(l=0)$	0 MeV	0 MeV
$V_{\rm o}(l=1)$	71.0752 MeV	43.6438 MeV
$V_{\rm so}(l=1)$	7.90622 MeV	7.84517 MeV
$V_{\rm o}(l=2)$	0 MeV	43.6438 MeV
$V_{\rm so}(l=2)$	0 MeV	0 MeV

TABLE IV. Parameters of the FHT interaction for GSM and GSM-CC calculations in ^{7}Li and ^{8}Li. For more details, see the caption of Table II.

Parameter	Value (MeV)
$\mathcal{V}^{\rm C}_{\rm t,t}$	4.03185
$\mathcal{V}^{\rm C}_{\rm s,t}$	–4.95286
$\mathcal{V}^{\rm C}_{\rm s,s}$	2.23361
$\mathcal{V}^{\rm C}_{\rm t,s}$	–7.63465
$\mathcal{V}^{\rm SO}_{\rm t,t}$	–1456.55
$\mathcal{V}^{\rm SO}_{\rm s,t}$	0
$\mathcal{V}^{\rm T}_{\rm t,t}$	15.4822
$\mathcal{V}^{\rm T}_{\rm s,t}$	–15.5716

value ($E_{\rm exp} = 10.948$ MeV). Reaction channels are obtained by the coupling of the ground state $3/2^-$ and the first excited state $1/2^-$ of ^{7}Li with the proton partial waves: $s_{1/2}$, $p_{1/2}$, $p_{3/2}$, $d_{3/2}$, and $d_{5/2}$.

Discrete states of a composite system ^{8}Li are 2^+_1 and 1^+_1 bound states, and 3^+_1 resonance. To correct for missing reaction channels in GSM-CC calculations, the channel-channel coupling potentials $V_{c,c'}$ have been modified and new potentials are $\tilde{V}_{c,c'} = c(J^\pi)V_{c,c'}$, with $c(2^+_1) = 1.03705$, $c(1^+_1) = 1.04805$, and $c(3^+_1) = 1.03205$.

B. ^{7}Li$(n,\gamma)^8$Li cross section

The neutron separation energy in the ground state of ^{7}Li is $S_{\rm n} = 7.25$ MeV. The final nucleus ^{8}Li has two bound states $J^\pi = 2^+_1$ and 1^+_1 below the neutron emission threshold. The calculated neutron separation energy from the ground state and the first excited states are $S^{\rm (th)}_{\rm n} = 2.032$ MeV and $S^{\rm (th)}_{\rm n} = 1.052$ MeV, respectively, in excellent agreement with the experimental data. The 3^+_1 resonance peak can be seen both in $M1$ and $E2$ transitions.

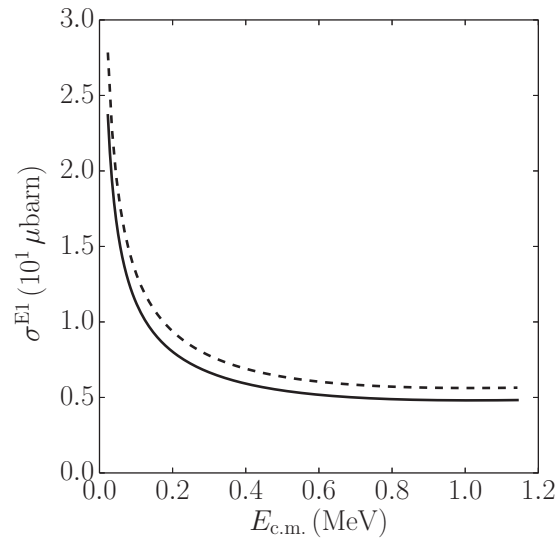

FIG. 7. The same as in Fig. 1 but for the ^{7}Li$(n,\gamma)^8$Li reaction. For more details, see the description in the text.

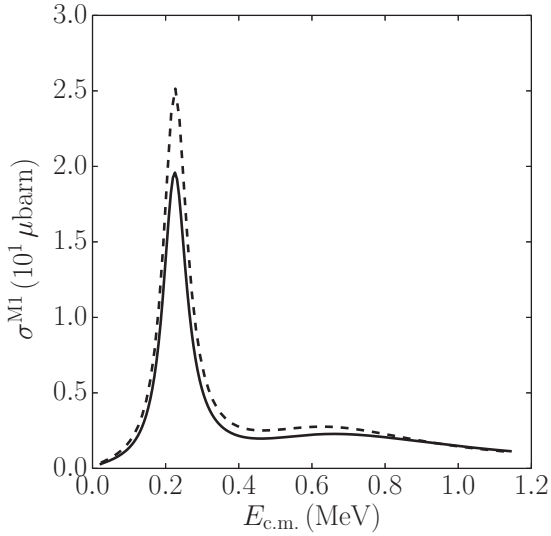

FIG. 8. The same as in Fig. 1 but for $M1$ transitions in the ^{7}Li$(n,\gamma)^8$Li reaction. The peak corresponds to the 3^+_1 resonance in ^{8}Li.

Figures 7–9 show the $E1$, $M1$, and $E2$ cross sections for ^{7}Li$(n,\gamma)^8$Li reaction. The solid lines in Figs. 7–9 show results of the fully antisymmetrized GSM-CC calculations with both ground and first excited states of ^{7}Li included. The dashed lines in these figures correspond to GSM-CC calculations neglecting the $1/2^-$ first excited state in ^{7}Li. Including the first excited state of the target lowers the $E1$ contribution to the neutron radiative capture cross section by $\sim$20% for $E_{c.m.} < 1$ MeV.

The $M1$ contribution to the cross section increases by $\sim$25% in the region of 3^+_1 resonance if the excited state of the target is included (see Fig. 8). One can see that the calculated 3^+_1 resonance is at the experimental value of energy $E_{c.m.} = 0.223$ MeV.

$E2$ transitions contribute very little to the neutron radiative capture cross section. The $E2$ contribution is three orders of magnitude smaller than $E1$ and $M1$ contributions. The role of the excited state of the target is very important. It increases the contribution from $E2$ transitions by a factor $\sim$3 in the region of 3^+_1 resonance. At the 1^+_2 resonance, the excited state enhances the $E2$ contribution by about one order of magnitude. The calculated energy of this resonance is lower than seen experimentally.

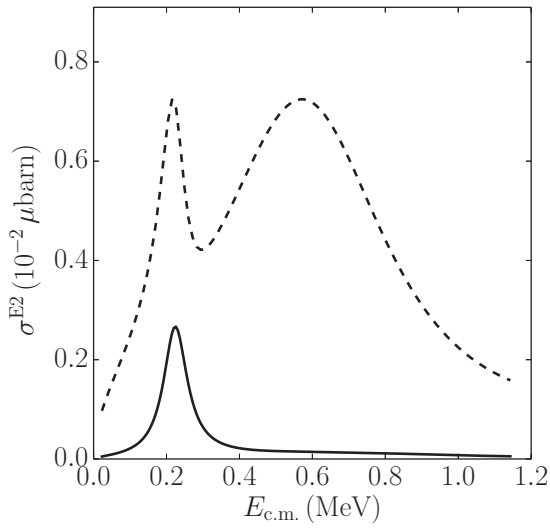

FIG. 9. The same as in Fig. 8 but for the $E2$ transitions. The two peaks correspond to the 3^+_1 and 1^+_2 resonances of ^{8}Li.

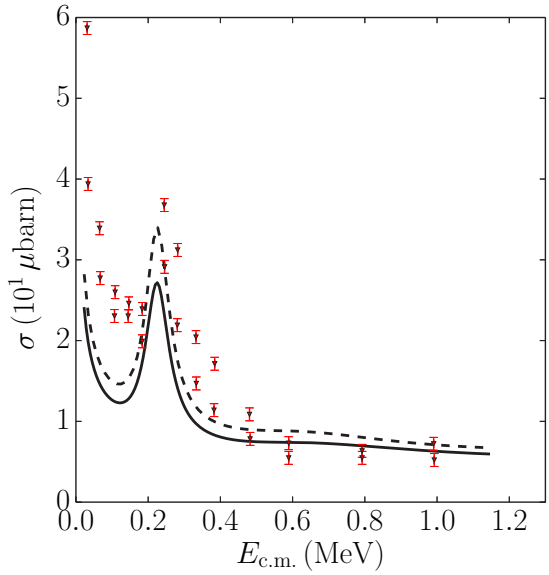

FIG. 10. (Color online) Plot of the total cross section for the ^{7}Li$(n,\gamma)^8$Li reaction. Data are taken from Ref. [62]. The solid line represents the exact, fully antisymmetrized calculation. Calculations in the long-wavelength approximation are represented by the dashed and dotted lines in the antisymmetrized and non-antisymmetrized cases, respectively. For more details see the description in the text.

The total neutron radiative capture cross section is compared with the experimental data [62] in Fig. 10. GSM-CC calculation underestimates the data of Imhof *et al.* [62]. The

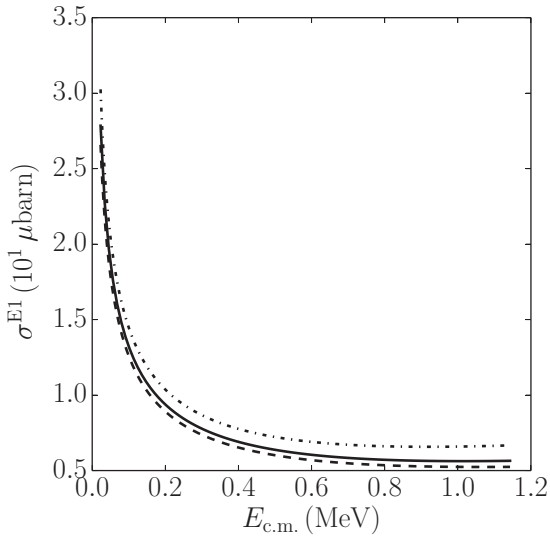

FIG. 11. The same as in Fig. 5 but for the ^{7}Li$(n,\gamma)^8$Li reaction. For more details, see the description in the text.

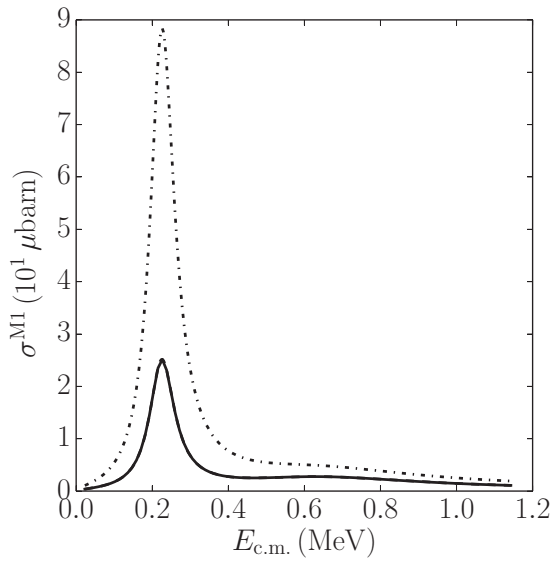

FIG. 12. The same as in Fig. 11 but for the $M1$ transitions. The peak corresponds to the 3_1^+ resonance in ^{8}Li.

extrapolation of the calculated neutron radiative capture cross section at low $E_{c.m.}$ is done using the expansion

$$\sigma(E_{c.m.}) = \frac{4.541}{\sqrt{E_{c.m.}}} - 2.360 + 3.387\sqrt{E_{c.m.}}, \qquad (68)$$

which yields $\sigma^{(\text{GSM-CC})} = 25.41$ μb at $E_{c.m.} = 25$ keV.

The long-wavelength approximation and the role of the antisymmetry of initial and final states in the calculation of matrix elements of the electromagnetic transitions is tested in Figs. 11 and 12. Only the ground state of ^{7}Li is taken into account in these tests. To correct GSM-CC calculations for the missing channels in this case, the channel-channel coupling potentials $V_{c,c'}$ have been corrected: $\tilde{V}_{c,c'} = c(J^\pi)V_{c,c'}$, and the multiplicative corrective factors are $c(2_1^+) = 1.038$, $c(1_1^+) = 1.0594$, and $c(3_1^+) = 1.032$.

At low energies ($E_{c.m.} < 1.2$ MeV), neither the long-wavelength approximation nor the antisymmetry of initial and final states in the calculation of $E1$ transition matrix elements change results significantly (see Fig. 11). Also $M1$ transition matrix elements are insensible to the long wavelength approximation (see Fig. 12). In contrast, the antisymmetrization is essential, decreasing the $M1$ contribution to the neutron radiative capture cross section by a factor ~ 4 in the region of 3_1^+ resonance.

VI. CONCLUSIONS

The GSM in the coupled-channel representation opens a possibility for the unified description of low-energy nuclear structure and reactions using the same Hamiltonian. While both GSM and GSM-CC can describe energies, widths, and wave functions of the many-body states, the GSM-CC can in addition yield reaction cross sections. Combined application of GSM and GSM-CC to describe energies of resonant states allows us to test the exactitude of calculated cross sections for a given many-body Hamiltonian.

In this work, we have presented in detail the GSM in the coupled channel representation and applied it to the description of the low-energy proton and neutron radiative capture processes on mirror targets ^{7}Be and ^{7}Li, respectively. The interaction between valence nucleons in this calculation was modeled by the finite-range two-body FHT interaction.

The convergence of GSM-CC calculations has been checked by comparing GSM and GSM-CC results for ^{8}B and ^{8}Li states. In a given single-particle model space, the GSM-CC calculation with the reaction channels which are constructed using selected many-body states of the target nucleus (^{7}Be or ^{7}Li in our case), can be considered reliable if the GSM-CC eigenvalues for a combined system (^{8}B or ^{8}Li in our case) approximate well the results of a direct diagonalization of the GSM Hamiltonian matrix in the same single-particle model space. In such a case, the configuration mixing in GSM-CC and GSM wave functions are equivalent and one does not need to include additional states of the target nucleus to reach the many-body completeness in the GSM-CC calculation. Only in this case, the unified description of nuclear structure and reactions with the same many-body Hamiltonian and the same model space is reached. In the studied case, the GSM and GSM-CC spectra were close but not identical, so the small renormalization of the channel-channel coupling potentials was necessary to compensate for the missing channels made of the higher-lying discrete and/or continuum states of the target. In the reactions involving heavier nuclei and/or higher c.m. energies, the number of channels is such that the unified description of structure and reactions with the same Hamiltonian is simply not conceivable.

There are two important aspects in this GSM-CC calculations which have been studied carefully. The first one is the antisymmetry of initial and final states in the calculation of matrix elements of the electromagnetic operators. It was found that the antisymmetry is crucial in $M1$ transitions in the region of resonances. At energies of astrophysical importance, the error introduced by neglecting the antisymmetry is, however, small. The second aspect is the role of the excited state $1/2^-$ of the target. At $E_{c.m.} \sim 0$, the radiative capture cross sections in ^{7}Be$(p,\gamma)^8$B and ^{7}Li$(n,\gamma)^8$Li reactions are slightly impacted by the excited state of the target. However, in the region of resonances and at higher energies the excited $1/2_1^-$ state in ^{7}Be and ^{7}Li turns out to be crucial. As compared to the ^{7}Be$(p,\gamma)^8$B reaction, the ^{7}Li$(n,\gamma)^8$Li reaction is less sensitive to the first excited state of the target but more sensitive to the antisymmetry of initial and final states in the calculation of matrix elements of electromagnetic transition operators. The long-wavelength approximation in the transition matrix elements changes mainly the $E1$ contribution to the radiative capture cross section.

ACKNOWLEDGMENTS

This work was supported partially through FUSTIPEN (French-US Theory Institute for Physics with Exotic Nuclei) under DOE Grant No. DE-FG02-10ER41700 and by the DOE Grant No. DE-FG02-97ER40963 (University of Tennessee).

APPENDIX: MATRIX ELEMENTS OF THE ELECTROMAGNETIC TRANSITION OPERATORS

The matrix elements related to electric and magnetic transitions will be considered with and without the long-wavelength approximation. The operators involving the exact and approximate electromagnetic field can be found in Ref. [63], whose matrix elements can be derived straightforwardly from the Wigner-Eckhart theorem and standard manipulations of gradients of spherical harmonics coupled to angular momenta [64]. The operator $\hat{\mathcal{M}}_{L,M_L}$ separates into electric $\hat{\mathcal{M}}^E_{L,M_L}$ and magnetic $\hat{\mathcal{M}}^M_{L,M_L}$ parts:

$$\hat{\mathcal{M}}^E_{L,M_L} = \sum_i e_i \frac{(2L+1)!!}{(L+1)k_\gamma^L}\left[S'_L(k_\gamma \hat{r}_i) + \frac{k_\gamma \hat{r}_i}{2} S_L(k_\gamma \hat{r}_i)\right]\hat{Y}^L_{M_L}(\Omega_i) + \sum_i e_i \frac{(2L+1)!!}{(L+1)k_\gamma^L}\frac{\hbar c}{2m_p c^2} g_i^s \left[\frac{S_L(k_\gamma \hat{r}_i)}{\hat{r}_i}\right](\hat{\vec{l}}_i \cdot \hat{\vec{s}}_i)\hat{Y}^L_{M_L}(\Omega_i), \tag{A1}$$

$$\begin{aligned}
\hat{\mathcal{M}}^M_{L,M_L} &= \frac{\hbar c}{2m_p c^2}\sum_i \frac{(2L+1)!!}{(L+1)k_\gamma^L}\left[g_i^l \vec{\nabla}_i\left(\frac{S_L(k_\gamma \hat{r}_i)}{k_\gamma \hat{r}_i}\hat{Y}^L_{M_L}(\Omega_i)\right)\cdot \hat{\vec{l}}_i + g_i^s \vec{\nabla}_i\left(S'_L(k_\gamma \hat{r}_i) Y^L_{M_L}(\Omega_i)\right)\cdot \hat{\vec{s}}_i\right] \\
&\quad + \frac{\hbar c}{2m_p c^2}\sum_i \frac{(2L+1)!!}{(L+1)k_\gamma^L} g_i^s (k_\gamma S_L(k_\gamma \hat{r}_i))\left(\hat{\vec{s}}_i \cdot \vec{u}_{r_i}\right)\hat{Y}^L_{M_L}(\Omega_i) \\
&= -\frac{\hbar c}{2m_p c^2}\sum_i \frac{(2L+1)!!}{(L+1)k_\gamma^L} g_i^l \sqrt{\frac{L+1}{2L+1}}\left(S'_L(k_\gamma \hat{r}_i) - \left(\frac{L+1}{\hat{r}_i}\right)\frac{S_L(k_\gamma \hat{r}_i)}{k_\gamma \hat{r}_i}\right)[\hat{\mathbf{Y}}^{L+1}(\Omega_i) \otimes \hat{\vec{l}}_i]^L_{M_L} \\
&\quad + \frac{\hbar c}{2m_p c^2}\sum_i \frac{(2L+1)!!}{(L+1)k_\gamma^L} g_i^l \sqrt{\frac{L}{2L+1}}\left(S'_L(k_\gamma \hat{r}_i) + \left(\frac{L}{\hat{r}_i}\right)\frac{S_L(k_\gamma \hat{r}_i)}{k_\gamma \hat{r}_i}\right)[\hat{\mathbf{Y}}^{L-1}(\Omega_i) \otimes \hat{\vec{l}}_i]^L_{M_L} \\
&\quad - \frac{\hbar c}{2m_p c^2}\sum_i \frac{(2L+1)!!}{(L+1)k_\gamma^L} g_i^s \sqrt{\frac{L+1}{2L+1}}\left[\left(\frac{L(L+1)}{(k_\gamma \hat{r}_i)^2} - 1\right)S_L(k_\gamma \hat{r}_i) - \left(\frac{L}{\hat{r}_i}\right)S'_L(k_\gamma \hat{r}_i)\right][\hat{\mathbf{Y}}^{L+1}(\Omega_i) \otimes \hat{\vec{s}}_i]^L_{M_L} \\
&\quad + \frac{\hbar c}{2m_p c^2}\sum_i \frac{(2L+1)!!}{(L+1)k_\gamma^L} g_i^s \sqrt{\frac{L}{2L+1}}\left[\left(\frac{L(L+1)}{(k_\gamma \hat{r}_i)^2} - 1\right)S_L(k_\gamma \hat{r}_i) + \left(\frac{L+1}{\hat{r}_i}\right)S'_L(k_\gamma \hat{r}_i)\right][\hat{\mathbf{Y}}^{L-1}(\Omega_i) \otimes \hat{\vec{s}}_i]^L_{M_L} \\
&\quad + \frac{\hbar c}{2m_p c^2}\sum_i \frac{(2L+1)!!}{(L+1)k_\gamma^L} g_i^s (k_\gamma S_L(k_\gamma \hat{r}_i))\left(\hat{\vec{s}}_i \cdot \vec{u}_{r_i}\right)\hat{Y}^L_{M_L}(\Omega_i),
\end{aligned} \tag{A2}$$

where i runs over all considered nucleons and $\hat{\vec{l}}_i$ and $\hat{\vec{s}}_i$ are the orbital and spin angular momenta, respectively. In the above expression, $\hat{Y}^L_{M_L}(\Omega)$ is a spherical harmonics, S_L is the Ricatti-Bessel function, $\hat{r}_i$ and Ω_i are radial and angular coordinates of the nucleon i, and $\vec{u}_{r_i} = \hat{\vec{r}}_i/\hat{r}_i$. Moreover, e_i is the dimensionless charge of the nucleon i ($e_i = 1$ for a proton and 0 for a neutron), g_i^s is the dimensionless magnetic spin moment of the nucleon i ($g_i^s = 5.5857$ for a proton and -3.8263 for a neutron), $m_p c^2$ (in units of MeV) is the mass of the proton, and g_i^l is the dimensionless magnetic orbital momentum of the nucleon i times $L+1$ ($g_i^l = 2$ for a proton and 0 for a neutron).

In the long-wavelength approximation, the expressions (A1) and (A2) become

$$\hat{\mathcal{M}}^E_{L,M_L} = \sum_i e_i \hat{r}_i^L \hat{Y}^L_{M_L}(\Omega_i), \tag{A3}$$

$$\begin{aligned}
\hat{\mathcal{M}}^M_{L,M_L} &= \frac{\hbar c}{2m_p c^2}\sum_i \left[\frac{g_i^l}{L+1}\vec{\nabla}_i\left(\hat{r}_i^L \hat{Y}^L_{M_L}(\Omega_i)\right)\cdot \hat{\vec{l}}_i + g_i^s \vec{\nabla}_i\left(r_i^L Y^L_{M_L}(\Omega_i)\right)\cdot \hat{\vec{s}}_i\right] \\
&= \frac{\hbar c}{2m_p c^2}\sum_i \sqrt{L(2L+1)}\hat{r}_i^{L-1}\frac{g_i^l}{L+1}[\hat{\mathbf{Y}}^{L-1}(\Omega_i) \otimes \hat{\vec{l}}_i]^{L_{M_L}} + \frac{\hbar c}{2m_p c^2}\sum_i \sqrt{L(2L+1)}\hat{r}_i^{L-1} g_i^s [\hat{\mathbf{Y}}^{L-1}(\Omega_i) \otimes \hat{\vec{s}}_i]^{L_{M_L}}.
\end{aligned} \tag{A4}$$

Equations (A1)–(A4) have been written in such a way that only one-body operators appear in each summation. Matrix elements of these operators are calculated in a standard way using the Wigner-Eckhart theorem.

[1] H. Feshbach, Ann. Phys. (NY) **19**, 287 (1962).
[2] H. Feshbach, Ann. Phys. (NY) **5**, 357 (1958).
[3] C. Mahaux and H. A. Weidenmüller, *Shell-Model Approach to Nuclear Reactions* (North-Holland, Amsterdam, 1969).
[4] H. W. Barz, I. Rotter, and J. Höhn, Nucl. Phys. A **275**, 111 (1977).
[5] K. Bennaceur, F. Nowacki, J. Okołowicz, and M. Płoszajczak, Nucl. Phys. A **671**, 203 (2000).

[6] A. Volya and V. Zelevinsky, Phys. Rev. C **74**, 064314 (2006).
[7] A. Volya and V. Zelevinsky, Phys. Rev. Lett. **94**, 052501 (2005).
[8] N. Michel, W. Nazarewicz, M. Płoszajczak, and K. Bennaceur, Phys. Rev. Lett. **89**, 042502 (2002).
[9] N. Michel, W. Nazarewicz, M. Płoszajczak, and J. Okołowicz, Phys. Rev. C **67**, 054311 (2003).
[10] N. Michel, W. Nazarewicz, M. Płoszajczak, and T. Vertse, J. Phys. G: Nucl. Part. Phys. **36**, 013101 (2009).
[11] Y. Jaganathen, N. Michel, and M. Płoszajczak, J. Phys.: Conf. Series **403**, 012022 (2012).
[12] Y. Jaganathen, N. Michel, and M. Płoszajczak, Phys. Rev. C **89**, 034624 (2014).
[13] R. I. Betan, A. T. Kruppa, and T. Vertse, Phys. Rev. C **78**, 044308 (2008).
[14] G. Papadimitriou, J. Rotureau, N. Michel, M. Płoszajczak, and B. R. Barrett, Phys. Rev. C **88**, 044318 (2013).
[15] E. G. Adelberger, A. Garcia, R. G. H. Robertson, K. A. Snover, A. B. Balantekin, K. Heeger, M. J. Ramsey-Musolf, D. Bemmerer, A. Junghans, C. A. Bertulani, J. W. Chen, H. Costantini, P. Prati, M. Couder, E. Uberseder, M. Wiescher, R. Cyburt, B. Davids, S. J. Freedman, M. Gai, D. Gazit, L. Gialanella, G. Imbriani, U. Greife, M. Hass, W. C. Haxton, T. Itahashi, K. Kubodera, K. Langanke, D. Leitner, M. Leitner, P. Vetter, L. Winslow, L. E. Marcucci, T. Motobayashi, A. Mukhamedzhanov, R. E. Tribble, K. M. Nollet, F. M. Nunes, T. S. Park, P. D. Parker, R. Schiavilla, E. C. Simpson, C. Spitaleri, F. Strieder, H. P. Trautvetter, K. Suemmere, and S. Typel, Rev. Mod. Phys. **83**, 195 (2011).
[16] B. W. Filippone, A. J. Elwyn, C. N. Davids, and D. D. Koetke, Phys. Rev. Lett. **50**, 412 (1983).
[17] B. W. Filippone, A. J. Elwyn, C. N. Davids, and D. D. Koetke, Phys. Rev. C **28**, 2222 (1983).
[18] F. Hammache, G. Bogaert, P. Aguer, C. Angulo, S. Barhoumi, L. Brillard, J. F. Chemin, G. Claverie, A. Coc, M. Hussonnois, M. Jacotin, J. Kiener, A. Lefebvre, J. N. Scheurer, J. P. Thibaud, and E. Virassamynaïken, Phys. Rev. Lett. **80**, 928 (1998).
[19] F. Hammache, G. Bogaert, P. Aguer, C. Angulo, S. Barhoumi, L. Brillard, J. F. Chemin, G. Claverie, A. Coc, M. Hussonnois, M. Jacotin, J. Kiener, A. Lefebvre, C. Le Naour, S. Ouichaoui, J. N. Scheurer, V. Tatischeff, J. P. Thibaud, and E. Virassamynaïken, Phys. Rev. Lett. **86**, 3985 (2001).
[20] A. R. Junghans, E. C. Mohrmann, K. A. Snover, T. D. Steiger, E. G. Adelberger, J. M. Casandjian, H. E. Swanson, L. Buchmann, S. H. Park, and A. Zyuzin, Phys. Rev. Lett. **88**, 041101 (2002).
[21] A. R. Junghans, E. C. Mohrmann, K. A. Snover, T. D. Steiger, E. G. Adelberger, J. M. Casandjian, H. E. Swanson, L. Buchmann, S. H. Park, A. Zyuzin, and A. M. Laird, Phys. Rev. C **68**, 065803 (2003).
[22] L. T. Baby, C. Bordeanu, G. Goldring, M. Hass, L. Weissman, V. N. Fedoseyev, U. Köster, Y. Nir-El, G. Haquin, H. W. Gäggeler, R. Weinreich, and the ISOLDE Collaboration, Phys. Rev. C **67**, 065805 (2003).
[23] L. T. Baby, C. Bordeanu, G. Goldring, M. Hass, L. Weissman, V. N. Fedoseyev, U. Köster, Y. Nir-El, G. Haquin, H. W. Gäggeler, R. Weinreich, and the ISOLDE Collaboration, Phys. Rev. Lett. **90**, 022501 (2003).
[24] L. T. Baby, C. Bordeanu, G. Goldring, M. Hass, L. Weissman, V. N. Fedoseyev, U. Köster, Y. Nir-El, G. Haquin, H. W. Gäggeler, R. Weinreich, and the ISOLDE Collaboration, Phys. Rev. C **69**, 019902(E) (2004).
[25] L. T. Baby, C. Bordeanu, G. Goldring, M. Hass, L. Weissman, V. N. Fedoseyev, U. Köster, Y. Nir-El, G. Haquin, H. W. Gäggeler, R. Weinreich, and the ISOLDE Collaboration, Phys. Rev. Lett. **92**, 029901(E) (2004).
[26] A. R. Junghans, K. A. Snover, E. C. Mohrmann, E. G. Adelberger, and L. Buchmann, Phys. Rev. C **81**, 012801(R) (2010).
[27] G. Baur, C. A. Bertulani, and H. Rebel, Nucl. Phys. A **458**, 188 (1986).
[28] N. Iwasa, F. Boué, G. Surówka, K. Sümmerer, T. Baumann, B. Blank, S. Czajkowski, A. Förster, M. Gai, H. Geissel, E. Grosse, M. Hellström, P. Koczon, B. Kohlmeyer, R. Kulessa, F. Laue, C. Marchand, T. Motobayashi, H. Oeschler, A. Ozawa, M. S. Pravikoff, E. Schwab, W. Schwab, P. Senger, J. Speer, C. Sturm, A. Surowiec, T. Teranishi, F. Uhlig, A. Wagner, W. Walus, and C. A. Bertulani, Phys. Rev. Lett. **83**, 2910 (1999).
[29] B. Davids, D. W. Anthony, T. Aumann, S. M. Austin, T. Baumann, D. Bazin, R. R. C. Clement, C. N. Davids, H. Esbensen, P. A. Lofy, T. Nakamura, B. M. Sherrill, and J. Yurkon, Phys. Rev. Lett. **86**, 2750 (2001).
[30] F. Schümann, F. Hammache, S. Typel, F. Uhlig, K. Sümmerer, I. Böttcher, D. Cortina, A. Förster, M. Gai, H. Geissel, U. Greife, N. Iwasa, P. Koczoń, B. Kohlmeyer, R. Kulessa, H. Kumagai, N. Kurz, M. Menzel, T. Motobayashi, H. Oeschler, A. Ozawa, M. Płoskoń, W. Prokopowicz, E. Schwab, P. Senger, F. Strieder, C. Sturm, Z.-Y. Sun, G. Surówka, A. Wagner, and W. Waluś, Phys. Rev. Lett. **90**, 232501 (2003).
[31] F. Schümann, S. Typel, F. Hammache, K. Sümmerer, F. Uhlig, I. Böttcher, D. Cortina, A. Förster, M. Gai, H. Geissel, U. Greife, E. Grosse, N. Iwasa, P. Koczoń, B. Kohlmeyer, R. Kulessa, H. Kumagai, N. Kurz, M. Menzel, T. Motobayashi, H. Oeschler, A. Ozawa, M. Płoskoń, W. Prokopowicz, E. Schwab, P. Senger, F. Strieder, C. Sturm, Z.-Y. Sun, G. Surówka, A. Wagner, and W. Waluś, Phys. Rev. C **73**, 015806 (2006).
[32] K. H. Kim, M. H. Park, and B. T. Kim, Phys. Rev. C **35**, 363 (1987).
[33] D. Halderson, Phys. Rev. C **73**, 024612 (2006).
[34] F. C. Barker, Nucl. Phys. A **588**, 693 (1995).
[35] K. Bennaceur, F. Nowacki, J. Okołowicz, and M. Płoszajczak, Nucl. Phys. A **651**, 289 (1999).
[36] P. Descouvemont, Phys. Rev. C **70**, 065802 (2004).
[37] P. Navrátil, R. Roth, and S. Quaglioni, Phys. Lett. B **704**, 379 (2011).
[38] J. H. Applegate, C. J. Hogan, and R. J. Scherrer, Phys. Rev. D **35**, 1151 (1987).
[39] G. M. Fuller, G. J. Mathews, and C. R. Alcock, Phys. Rev. D **37**, 1380 (1988).
[40] R. A. Malaney and W. A. Fowler, Astrophys. J. **333**, 14 (1988).
[41] N. Terasawa and K. Sato, Prog. Theor. Phys. **81**, 1085 (1989).
[42] M. Wiescher, R. Steininger, and F. Käppeler, Astrophys. J. **344**, 464 (1989).
[43] M. Heil, F. Käppeler, M. Wiescher, and A. Mengoni, Astrophys. J. **507**, 997 (1998).
[44] Y. Nagai, M. Igashira, T. Takaoka, T. Kikuchi, T. Shima, A. Tomyo, A. Mengoni, and T. Otsuka, Phys. Rev. C **71**, 055803 (2005).
[45] R. Izsák, Á. Horváth, Á. Kiss, Z. Seres, A. Galonsky, C. A. Bertulani, Z. Fülöp, T. Baumann, D. Bazin, K. Ieki, C. Bordeanu, N. Carlin, M. Csanád, F. Deák, P. DeYoung, N. Frank, T. Fukuchi, A. Gade, D. Galaviz, C. R. Hoffman, W. A. Peters,

H. Schelin, M. Thoennessen, and G. I. Veres, Phys. Rev. C **88**, 065808 (2013).
[46] C. Wang, O. I. Cissé, and D. Baye, Phys. Rev. C **80**, 034611 (2009).
[47] S. B. Dubovichenko, Phys. At. Nucl. **76**, 841 (2013).
[48] P. Descouvemont and D. Baye, Nucl. Phys. A **567**, 341 (1994).
[49] G. Rupak and R. Higa, Phys. Rev. Lett. **106**, 222501 (2011).
[50] Y. Suzuki and K. Ikeda, Phys. Rev. C **38**, 410 (1988).
[51] R. D. Lawson, *Theory of the Nuclear Shell Model* (Clarendon Press, Oxford, 1980).
[52] H. J. Lipkin, Phys. Rev. **110**, 1395 (1958).
[53] R. R. Whitehead, A. Watt, B. J. Cole, and I. Morrison, Adv. Nucl. Phys. **9**, 123 (1977).
[54] H. Furutani, H. Horiuchi, and R. Tamagaki, Prog. Theor. Phys. **60**, 307 (1978).
[55] H. Furutani, H. Horiuchi, and R. Tamagaki, Prog. Theor. Phys. **62**, 981 (1979).
[56] T. Berggren, Nucl. Phys. A **109**, 265 (1968).
[57] R. M. Id Betan, A. Rácz, and T. Vertse, Int. J. Theor. Phys. **50**, 2222 (2011).
[58] N. Michel, Eur. Phys. J. A **42**, 523 (2009).
[59] R. M. Id Betan, Phys. Lett. B **730**, 18 (2014).
[60] W. F. Hornyak, *Nuclear Structure* (Academic Press, New York, 1975).
[61] A. Bohr and B. R. Mottelson, *Nuclear Structure, Vol. 2: Nuclear Deformations* (World Scientific, Singapore, 1998).
[62] W. L. Imhof, R. G. Johnson, F. J. Vaughn, and M. Walt, Phys. Rev. **114**, 1037 (1959).
[63] A. de Shalit and I. Talmi, *Nuclear Shell Theory* (Dover Publications, Mineola, NY, 2004).
[64] D. A. Varshalovich, A. N. Moskalev, and V. K. Khersonskii, *Quantum Theory of Angular Momentum* (Sciences, Leningrad, 1975).